

First, we would like to thank the editor and the two anonymous referees for their valuable and relevant comments. Our replies are found below.

Authors' corrections to the manuscript

Besides answering the questions from the referees we have also made some editing to the manuscript:

We have made some editorial changes for English usage (Nothing major, just a bit of native-speaker polish.).

The Abstract and parts of the Introduction have been rewritten to pinpoint the manuscript's contributions.

Page 8, line 26 and line 27. The reference of Christensen et al (2015) was an old HESSD reference. The manuscript has now been published and is therefore cited as Christensen et al (2016).

Page 17 line 21-22: To clarify, " On the contrary, SHI models..." has been changed to " On the contrary, SHI-sharp models..."

Page 19 line 3: We have corrected the statement "The superiority of SHI-smooth-3 models..." to "The superiority of SHI-sharp-3 models..."

Page 21 line 16-17: We have corrected the statement "... and therefore the sensitivity is concentrated in the more resistive layers." to "... and therefore the sensitivity is concentrated in the less resistive layers."

Fig. 3. Y-label has been corrected, and some additional text has been added to the figure caption.

Fig. 7. To clarify we have updated the figure text and the caption from "SHI-smooth" to "SHI-smooth-3" and from "SHI-sharp" to "SHI-sharp-3".

Fig. 9. We have updated the text in the caption, because the order of predictions (the columns) in the figure did not correspond to the caption text.

Referee #1: The author's response and corrections

Comments from Referee # 1	Authors Comments	Changes in manuscript
<p>General comments 1. <i>In section 3.3, depth and direction dependent horizontal constraint factors were used for both smooth and sharp inversions, and the constraint factors assigned for the two inversion methods are different. However, in the results part, the author compared the impact of the two methods on the predictions of flow model, is the comparison fair?</i></p>		<p>Yes, the reviewer is right. This section was not clear enough. We have added a few more sentences about our choice of constraint factors and how these were determined.</p>
<p>General comments 2. <i>In section 3.4, the author weighted the river discharge observation more than hydraulic head observation when defined the objective function. Why the author think that the calibrated models have error in their simulation of hydraulic head but not in simulation of river discharge?</i></p>		<p>We have rewritten the explanation of our choice of weights that follows after equation (7).</p>
<p>General comments 3. <i>Figure 1 in this manuscript described the conceptual flowchart for the sequential hydrogeophysical inversion. The whole framework of the experiment process was clearly displayed by the flowchart, however the content and details of each experiment step are obscure. It is hard to understand that what kind of experiment was conducted exactly in this research without reading the text description, thus I suggest the author modify the flowchart to make it intelligible.</i></p>	<p>We don't understand? However, some references to the flowchart in the body text of the manuscript could be clearer and consistent with the numbering!</p>	<p>We have made a few improvements to figure 1 to clarify the workflow. Page 7 line 10: (Error! Reference source not found., box 1) changed to (figure 1, box 2)</p>

Referee #2: The author's response and corrections

Comments from referee # 2	Authors Comments	Changes in manuscript
<p><i>This paper uses geophysical “voxel inversion” to do resistivity field estimation, and linked the resistivity field with hydraulic conductivity field through power law. Those methods are already proposed and utilized in the past. Please highlight the new theoretical development and findings.</i></p>	<p>This paper is the first to demonstrate application of voxel inversion results directly in a groundwater modeling context. Furthermore, it presents and demonstrates a novel parameterization method for a groundwater model for which the calibration is supported by the 3D geophysical voxel model. Finally, it demonstrates the importance of choosing a geologically plausible regularization when the geophysical model is to be used in a groundwater modeling context. Furthermore, it should also be pointed out that previous studies (linking resistivity field with hydraulic conductivity field through a power law) that we cite deal with interpretation of tomographic data that provide a high degree of resolution, thereby allowing for interpretation of spatial variability in petrophysical relationships. In large scale applications (ten to thousands of square kilometers), this type of data will in general not be available.</p>	<p>We have rewritten parts of the Abstract.</p> <p>On page 4 L25-28 we added this sentences in the text: <i>“However, it is often ignored that geophysical data can be inverted using alternative regularization schemes, and to test whether the alternative geophysical models affect the predictive capability of a groundwater model.”</i></p>
<p><i>In the numerical part, all the simulations are done with pre-defined true/reference model without the realistic field data. It will be better to prove the idea with realistic field data than the synthetic model.</i></p>	<p>We disagree with the referees saying that “it will be better to prove the idea with realistic field data than the synthetic model”. Nothing can be “proved” from a real field case using real data; this can only be used to “demonstrate” that the method can be applied in practice and that it can produce results that appear to be plausible. The results from a real field case can only be evaluated by subjective plausibility. This fact is actually our reason for using a</p>	<p>Nothing changed in the manuscript</p>

	<p>synthetic model with “realistic complexity” and “synthetic data sets” that are comparable to typical data sets for a real field case. Using the synthetic case makes us able to compare model estimation results and predictions with “true fields” and “true values of the predictions”. By using the synthetic case we can quantify actual estimation errors and actual prediction errors; we can for example quantify the improvement obtained by using sharp instead of smooth inversion.</p> <p>Furthermore, in this case, we have tried to faithfully represent the standard practice of hydrologists in constructing models (first handling the geophysical data, hereafter the geophysical models are used as input to the hydrological construction/calibration)</p>	
<p><i>In the section 3.3, how do you get those values of constraint factors?</i></p>	<p>This answer has also been given to referee #1:</p>	<p>Yes, the reviewer is right. This section was not clear enough. We have added a few more sentences about our choice of constraint factors and how these were determined.</p>
<p><i>In the section 3.4, the choices of weights for head and discharge data are significantly different. Why it has such a big difference? In the reality, how could you get the weight based on “trial and error” method?</i></p>	<p>This answer has also been given to referee #1:</p> <p>We can add a few more sentences about our choice of weights to the manuscript if this is recommended.</p>	<p>As said above to referee #1, we have rewritten the explanation of our choice of weights that follows after equation (7).</p>
<p><i>In the simulation part, the only case used Smooth regularization is Smooth-3. What is the simulation results looks like for other noise level?</i></p>	<p>Good question! We did not analyze other smooth models than “smooth-3”, because when we saw the “smooth-3” and “sharp-3” results it convinced us that for the studied case the smooth model will always perform worse than the sharp model. This is because the geology of the synthetic system consists of</p>	<p>Nothing changed</p>

	<p>“large-scale” structures of categorical fields with sharp transitions (like in a North-European or North-American glacial landscape). “Smooth inversion” cannot produce sharp transitions, so it is unlikely that a “smooth model” can do as good as a “sharp model”. We therefore only use the one “smooth-3” example to demonstrate ramifications of using smooth instead of sharp inversion. We do not see value in performing the comparison for other noise levels. Furthermore, doing the remaining smooth simulations would be computationally expensive (approx. 2-3 weeks using 64 CPU’s).</p>	
--	--	--

Voxel inversion of airborne electromagnetic data for improved groundwater model construction and prediction accuracy

N. K. Christensen¹, and T.P.A Ferre², G. Fiandaca¹, S. Christensen¹

[1]{Department of Geoscience, Aarhus University, Aarhus,Denmark}

[2]{Department of Hydrology and Water Resources, University of Arizona, Tucson, USA.}

Correspondence to: N. K. Christensen (phda.nikolaj.kruse@geo.au.dk)

Abstract

We present a workflow for ~~automated~~efficient construction and calibration of large-scale groundwater models that includes the integration of airborne electromagnetic (AEM) data and hydrological data. In the first step, ~~The~~ AEM data are inverted to form a 3D geophysical model. ~~The parameter of interest is the hydraulic conductivity, which can be determined by translating~~ In the second step, the 3D geophysical model is translated, using a spatially dependent petrophysical relationship, to form a 3D hydraulic conductivity distribution. ~~We use~~ The geophysical models and the hydrological data are used to estimate ~~determine the optimum~~ spatially distributed petrophysical ~~relationship~~shape factors. The ~~two~~ shape factors ~~of the petrophysical relationship~~ primarily work as translators between resistivity and hydraulic conductivity, but ~~the shape factors~~ they can also compensate for structural defects in the geophysical model.

The method is demonstrated for a synthetic case study with sharp transitions ~~between~~among various types of deposits. Besides demonstrating the methodology, we demonstrate the importance of using geophysical regularization constraints that conform well with the depositional environment. This is done by inverting ~~e-the~~ AEM data are inverted using either with both smoothness (smooth) constraints and/or minimum gradient support (sharp) constraints, where the use of sharp constraints conform best with the environment, resulting in two competitive geophysical models. The ~~value of the dependency on~~ AEM data quality is also tested by inverting the ~~alternative~~ geophysical models using data corrupted with four different levels of background noise. Subsequently, the geophysical models are used to construct ~~two~~ competing groundwater models for which the shape factors are calibrated. The performance of ~~the each flow groundwater~~ model was is tested ~~for~~ with respect to four types of prediction. ~~All predictions occurred that are~~ beyond the calibration base. Predictions of a pumping

1 well's recharge area and groundwater age, respectively, were are predicted by applying the same stress
2 situation as applied during for the hydrologic model calibration, while predictions of and head and
3 stream discharge was done are predicted for a different stress situation changed from those applied
4 during hydrologic model calibration.

5 As expected, in this case the predictive capability of a groundwater model is better when it is based on
6 a sharp geophysical model instead of a smoothness constraint. This is true for predictions of recharge
7 area, head change, and stream discharge, while we find no improvement for prediction of groundwater
8 age. The results show that geophysical models inverted with sharp constraints improve the predictive
9 capability of the groundwater models compared to geophysical models inverted with smooth
10 constraints. It was found that the use of sharp models improves the prediction of recharge area, while
11 prediction of groundwater age does not improve significantly. When the stress situation is changed the
12 prediction of head change and stream discharge improves significantly for sharp models compared to
13 smooth models. This is especially true for predictions of head change made in the vicinity of the
14 pumping well and far away from hydrologic boundaries. Furthermore, we show that the geophysical
15 data quality has variable influence on different model predictions. Prediction the model prediction
16 accuracy improves with AEM data quality for predictions of recharge area, head change and stream
17 discharge, while the accuracy there appears to be not accuracy improvement for the prediction of
18 groundwater age.

19 **1 Introduction**

20 Large-scale geological and groundwater models are used extensively to support aquifer management.
21 (Here “large scale” refers to an area of from tens to thousands of square kilometers.) Determining the
22 distribution of hydraulic properties and the geometry and connectivity of the groundwater system is of
23 significant importance since because these features control the flow paths (Desbarats and Srivastava
24 1991; Fogg et al. 1999; Weissmann and Fogg 1999). Incorrect reconstruction of the geological
25 structures has thus been recognized as an the most important source of uncertainty when a
26 groundwater model is used to make predictions outside its calibration base (Refsgaard et al. 2012;
27 Seifert et al. 2012; Zhou et al. 2014). The data traditionally used for structural mapping include
28 lithological logs from boreholes, hydrological data, and hydraulic testing results, but these data are
29 often sparse and unevenly distributed within an investigated domain. In these (very common) cases,
30 data scarcity becomes a major obstacle for structural mapping in relation to large scale groundwater
31 modeling (Refsgaard et al. 2012; Zhou et al. 2014).

32 Ground-based and airborne electromagnetic method (AEM) methods have shown a great potential for
33 mapping of geological structures (Jørgensen et al. 2003; Thomsen et al. 2004; Abraham et al. 2012;

1 Oldenborger et al. 2013; He et al. 2014; Munday et al. 2015). For large scale mapping, the airborne
2 electromagnetic method (AEM) is ~~an~~ efficient and cost-effective, supplementing method by which the
3 traditional data ~~can be supplemented by~~ with dense estimates of electrical resistivity which, in some
4 environments, inform about the lithology and thereby about structure (Robinson et al. 2008; Binley et
5 al. 2015). ~~The~~ AEM measurements can ~~quickly~~ be made quickly over large areas, and the resolution
6 can be as fine as 25 m in the horizontal direction and 5 m in the vertical (Schamper et al. 2014) with a
7 penetration depth of up to several hundred meters (Siemon et al. 2009).

8 Various methods ~~have been reported for how~~ to incorporate resistivity estimates (~~hereafter from now~~
9 ~~on-called~~ referred to as resistivity models) in groundwater model construction have been reported.
10 Manual and ~~knowledge-~~ knowledge-driven approaches have been used to combine geological,
11 hydrological and geophysical data with expert knowledge (Jørgensen et al. 2013). However, the
12 manual approach is subjective and ~~possibly can be~~ very time consuming and expensive to use when
13 resistivity models from large AEM surveys are to be incorporated in model construction.
14 Alternatively, more objective and cost-efficient geostatistical modeling approaches (Carle and Fogg
15 1996; Deutsch and Journel 1998; Strebelle 2002) are available for generating models from a
16 combination of borehole information and ~~AEM-AEM-~~ AEM- determined resistivity models. For example: He
17 et al. (2014) used a transition probability indicator simulation approach (Carle and Fogg 1996), while
18 Gunnink and Siemon (2015) used sequential indicator simulation (Deutsch 2006). Marker et al. (2015)
19 used a deterministic strategy for the integration of AEM resistivity models into the hydrological
20 modeling process.

21 The just mentioned studies all used sequential hydrogeophysical inversion approaches (SHI; as
22 defined by Ferré et al. 2009). In SHI the geophysical data are inverted first and independently from the
23 later inversion of the hydrological data. For large scale groundwater modeling, Herckenrath et al.
24 (2013) and Christensen et al. (2016) ~~were using-~~ used both SHI and joint hydrogeophysical inversion
25 approaches (JHI; as defined by Ferré et al. 2009). ~~By-~~ In JHI, the geophysical and hydrological data are
26 inverted jointly by linking the geophysical and hydrological models directly through some of their
27 parameters. The linking can, for example, be done by using an Archie's law inspired petrophysical
28 relationship (Archie 1942) to translate between the geophysical and hydrologic parameters.

29 In general, petrophysical relationships are difficult to establish, because such translation tends to be
30 site-, scale- and ~~facies-~~ facies- specific (Chen et al. 2001; Hyndman and Tronicke 2005; Slater 2007)
31 and uncertain (Mazáč et al. 1985; Slater 2007). The studies by Herckenrath et al. (2013) and
32 Christensen et al. (2016) ~~were using-~~ used a fixed petrophysical relationship throughout the model
33 domain. Better results can ~~potentially~~ be obtained by using a spatially variable relationship, which

1 allows for local translation between hydraulic conductivity and electrical resistivity, and by including
2 the spatially dependent petrophysical parameters in the optimization process (Linde et al. 2006).

3 There are two other challenges for incorporating resistivity models into large scale groundwater
4 modeling: differences in model discretization, and choice of geophysical regularization methodology.
5 Groundwater models are often discretized in a regular voxel grid while the traditional resistivity
6 models are 1D and placed at the respective sounding location. For airborne surveys, for example, the
7 resistivity models are normally located along the flight lines (Christiansen et al. 2006). Such resistivity
8 models therefore need to be relocated to conform to the grid of the groundwater model. The relocation
9 will often be a subtle process where information ~~easily~~ can be lost. To ~~accommodate~~ address this
10 issue, Fiandaca et al. (2015) presented a geophysical modeling approach referred to as “voxel
11 inversion”, which decouples the geophysical inversion model space from the geophysical
12 measurement positions. This allows estimation of a 3D geophysical model that is discretized on the
13 same voxel grid as the groundwater model.

14 Traditionally, geophysical regularization includes horizontal and vertical smoothing constraints
15 (Constable et al. 1987) or is limited to a ~~few-few~~-layer inversion (Auken and Christiansen 2004),
16 whereas a groundwater system often has sharp layer or body boundaries. It has therefore been
17 recognized, e.g. by Day-Lewis (2005) and others, that the regularization used to stabilize the
18 geophysical inversion may not reflect the actual hydrologic conditions unless it is chosen carefully. If,
19 for example, smooth regularization is used to estimate resistivity models in a sharply layered system, it
20 will produce a blurred resistivity distribution from which one should be careful with inferring the
21 spatial distribution of hydraulic conductivity to be used in a groundwater model. In this case, it would
22 be better to use minimum gradient support regularization (Portniaguine and Zhdanov 1999; Blaschek
23 et al. 2008; Vignoli et al. 2015) for the geophysical inversion because ~~thus the~~ estimated resistivity
24 distribution will tend to consist of fewer, ~~and~~ more sharply defined layer boundaries (vertically and
25 horizontally). However, it is often ignored that geophysical data can be inverted using alternative
26 regularization schemes, and to test whether that the alternative geophysical models are likely to lead
27 the alternative interpretations and conceptualizations of the hydrological system which may affect the
28 predictive capability of a groundwater model.

29
30 The main objective of the present study is to present a novel ~~In this paper we present a~~ sequential
31 hydrogeophysical approach ~~for using whereby~~ a voxel based 3D resistivity model is used to
32 parameterize and calibrate a groundwater model. ~~We will demonstrate that~~ The model
33 parameterization methodology allows the calibration to compensate for errors in the resistivity model.

1 | ~~Groundwater flow simulation of course depends on the alternative hydrogeological model on which it~~
2 | ~~is based. Therefore~~Furthermore, ~~we~~We will ~~also~~demonstrate that it is important for groundwater
3 | ~~modeling flow simulations~~ that the underlying resistivity model is estimated ~~by using~~regularization
4 | constraints that conform well to the geological environment. Finally, we analyze how groundwater
5 | model prediction accuracy depends on the quality of the geophysical data that was used to estimate the
6 | resistivity model. Section 2 of the paper presents the methodology. Section 3 describes the synthetic
7 | test case used for our demonstration purposes. Section 4 presents the results, while sections 5 and 6
8 | ~~present discusses discussions and conclusions of the work and draws the conclusions~~, respectively.
9 |
10 |

2 Methodology

Conceptually, ~~the methodology we~~ defines a translator function that describes the petrophysical relationship between electrical resistivity and hydraulic conductivity. ~~The A fundamental aspect is that~~ ~~the~~ petrophysical relationship can vary horizontally and vertically, thereby adapting to the local conditions in translation from the geophysical model space to the hydrological model space. Through inversion, the 3D spatially dependent optimal parameters of the petrophysical relationship are estimated for each layer interval, thereby covering the entire three-dimensional model space.

~~Figure 1~~ ~~Figure 1~~ provides a workflow for the method. First, the gathered airborne electromagnetic (AEM) data from the survey area are inverted with smooth or sharp horizontal and vertical constraints (Vignoli et al. 2015). This is done by using a recently developed voxel inversion scheme which decouples the geophysical model from the position of the acquired data (Fiandaca et al. 2015). The geophysical model space thus corresponds to the full 3D hydrological model grid. Secondly, the geophysical voxel based resistivity model is used as input for the ~~sub~~sequent hydrological inversion. The geophysical model parameter (resistivity) is linked to the main investigated parameter (hydraulic conductivity) through a petrophysical relationship ~~which that~~ has unknown shape factor values. The shape factor values are estimated through a hydrological inversion which minimizes an objective function describing the misfit between simulated groundwater model responses and corresponding observed hydrological data. Finally, the calibrated groundwater model can be used to make a set of relevant hydrologic predictions. The various steps of the methodology are explained in more detail in the following.

21

2.1 Geophysical voxel inversion

~~In the first step (Figure 1, box 1), T~~ the AEM data undergoes constrained deterministic inversion ~~(Figure 1, box 1)~~ using a recently developed voxel inversion approaches. This approach allows the geophysical model spaces to be spatially decoupled from the geophysical measurement positions (Fiandaca et al. 2015). In most inversion schemes, ~~the forward and inverse formulations use the same model discretization.~~ ~~for both inversion and forward calculation, but i~~ In the voxel formulation, the two model discretizations are decoupled. The voxel model space thus defines the geophysical properties on ~~the a set of~~ nodes of a regular 3D grid.

For calculating the forward responses, a “virtual” 1D model is a built at each sounding position. The “virtual” 1D model is defined by a number of layers, and layer thicknesses. The geophysical properties are interpolated from the voxel model space into the layer centers of the virtual model that is subsequently used to simulate the forward response for the corresponding sounding.

1 The voxel inversion approach thus allows for ~~inverting inversion of~~ AEM data into a geophysical
2 model defined on a 3D regular grid, regardless of the sounding positions. ~~This implies that~~ As a result,
3 the geophysical inversion can be conducted using the same grid as that defined for a 3D groundwater
4 model, ~~thereby minimizing.~~ S scaling issues in the coupling of geophysical and hydrological models
5 ~~can thus be avoided by using the same spatial discretization.~~

6 The general solution to the non-linear geophysical inversion problem can be found in Auken et al.
7 (2014). To stabilize the inverse problem, either of two types of regularization methods can be applied.
8 The first regularization method is commonly referred to as smoothness-constrained inversion
9 (Constable et al. 1987). The smoothness-constrained inversion tends to reduce contrasts and the
10 resulting geophysical model may appear blurred. The reason for this is found in its minimum-structure
11 L2 norm inversion formalism (Constable et al. 1987; Menke 2012). ~~F,~~ which following the notation
12 used by Vignoli et al. (2015), this can be expressed as:

$$(m_i - m_j)^2 / \sigma_{i,j}^2 \quad (1)$$

13 where the m_i and m_j are the constrained parameters and $\sigma_{i,j}$ defines the constraint strength. The
14 penalization of structures is clearly seen in eq. ~~(1)~~~~(1)~~, where $(m_i - m_j)^2 / \sigma_{i,j}^2$ is proportional to
15 the square of the value of the variation $(m_i - m_j)$. This implies that an increase in model parameter
16 variation will always result in a penalization in the stabilizer. The smoothness regularization thus
17 prevents reconstruction of sharp transitions.
18

19
20 The second regularization method is the minimum gradient support (Portniaguine and Zhdanov 1999;
21 Blaschek et al. 2008; Vignoli et al. 2015), which allows for large sharp vertical and horizontal model
22 transitions. The minimum gradient support regularization seeks to minimize the spatial variations
23 vertically and laterally by penalizing the vertical and horizontal model gradients through the stabilizer
24 expressed as (Vignoli et al., (2015)):

$$\frac{(m_i - m_j)^2 / \sigma_{i,j}^2}{(m_i - m_j)^2 / \sigma_{i,j}^2 + 1} \quad (2)$$

25

1 In eq. (2), $\sigma_{i,j}$ is a parameter used to control the sharpness of the regularization constraints. The
2 stabilizer contribution to the objective function is thus one when $|m_i - m_j| \gg \sigma_{i,j}$ and zero when
3 $\sigma_{i,j} \gg |m_i - m_j|$. The minimum gradient support functional thus counts the number of model
4 variations larger than $\sigma_{i,j}$ for the stabilizer term of the objective function. This formalism ~~thus~~ allows
5 sharp vertical and horizontal model transitions, which are ~~excessively~~ penalized excessively by the
6 smoothness-constrained inversion.

7

8 2.2 Hydrological model parametrization

9 ~~Section 2.1 describes an inversion methodology for which the geophysical property distribution can be~~
10 ~~estimated for each element in a voxel grid. In the second step- (Figure 1, box 12), -T~~the three
11 dimensional distribution of electrical resistivity values is linked to the ~~main investigated~~ hydrological
12 parameters (*e.g.* hydraulic conductivity) through a spatially varying petrophysical relationship.
13 Shape factors of this relationship are calibrated.

14 Linking hydraulic conductivity and electrical resistivity is not trivial because the parameter values and
15 the form of the petrophysical relationship may vary dramatically between different types of
16 environments. In addition, there can be fundamental questions about how the effective properties
17 controlling electrical current flow are related to the effective properties controlling fluid flow (Slater
18 2007). The primary factors controlling this relationship are porosity, pore water conductivity,
19 tortuosity, grain size, degree of saturation, amount of clay minerals, etc. (McNeill 1980). The simplest
20 petrophysical relationship is the empirical relationship known as Archie's law (Archie 1942), ~~that~~
21 which relates porosity, pore water conductivity, and the degree of saturation to bulk electrical
22 conductivity. However, this type of relationship does not take the electrical surface conductance ~~on the~~
23 ~~surface~~ of clay minerals into account. The Waxman and ~~Smith-Smits~~ model (Waxman and Smits
24 1968) combined with the dual-water model by Clavier et al. (1984) provides a basis for establishing
25 empirical relationships for shaly sand and sediments containing clays (Revil and Cathles 1999; Revil
26 et al. 2012). For glacial sedimentary environments, it is reported that clay has low electrical resistivity
27 and also low hydraulic conductivity, and sand has high electrical resistivity and high hydraulic
28 conductivity (Mazáč et al. 1985). For these environments, ~~it~~ is common to use a power law
29 relationship which is given some theoretical support by Purvance and Andricevic (2000). The
30 relationship is expressed as

$$K = \alpha \cdot \rho^\beta \quad (3)$$

31

1 where K is the hydraulic conductivity (m/s), ρ is the electrical resistivity (ohm-m), and α and β are
 2 two empirical shape factors. To compute K for each element in the groundwater model grid, α and β
 3 need to be parameterized and estimated. We suggest to make the parameterization by pilot points
 4 placed in a regular grid in each layer of the groundwater model (Certes and De Marsily 1991; Doherty
 5 2003). Each pilot point holds a set of α and β parameters, and kriging is used for spatial interpolation
 6 of α and β from the pilot points to the model grid. This kind of parametrization creates smooth
 7 transitions in the parameter fields and allows for variation in both the horizontal and vertical direction
 8 of the ρ to K translation. Hydraulic conductivity can thus be calculated by eq. ~~(3)~~ for every
 9 element in the groundwater model grid.

10

11 2.3 Hydrological Inversion

12 The model parameters, α and β at the pilot points, are calibrated by fitting the groundwater model to
 13 hydrological data. When the number of model parameters is large compared to the number of
 14 observation data, the minimization must be stabilized by regularization. The total objective function
 15 to be minimized is therefore a balanced compromise between a measurement term (Φ_m) and a
 16 regularization term (Φ_r). The combined objective function has the form

$$\Phi_{total} = \Phi_m + \mu \cdot \Phi_r = \sum_{i=1}^{n_d} \omega_{d,i} (d_{obs,i} - d_{sim,i})^2 + \mu \cdot \Phi_r \quad (4)$$

17

18 where Φ_{total} is the total objective function, $d_{obs,i}$ and $d_{sim,i}$ are measured and equivalent simulated
 19 data values, ω_{di} is a data dependent weight, μ is a weight factor, and ϕ_r is a Tikhonov regularization
 20 term. Here, ϕ_r is defined as preferred difference regularization, where the preferred difference
 21 between neighboring parameter values is set to zero. Φ_{total} is minimized iteratively, and the
 22 regularization weight factor, μ , is calculated during the iteration ~~in a way so to ensure that~~ Φ_m , the
 23 measurement part of the objective function, becomes approximately equal to a user specified target
 24 value (Doherty 2010).

25

26 3 Synthetic example

27 For illustrative purposes, we use a three dimensional synthetic system very similar to that presented by
 28 ~~Christensen et al. (2015)~~ Christensen et al. (2016). The only difference is that the active part of the

1 groundwater system only consists of 5 layers whereas ~~Christensen et al. (2015)~~ Christensen et al.
2 ~~(2016)~~ used a 20 layer model.

3 **3.1 Groundwater reference system and hydrological data**

4 The groundwater system is intended to mimic a glacial landscape and covers an area that is 7000 m
5 (N-S) by 5000 m (E-W). The geology of the system was generated using T-PROGS (Carle 1999) as
6 having a horizontal discretization of 25 m x 25 m, and a vertical discretization of 10 m. The system
7 extends 50 m in the vertical direction where it reaches impermeable clay with a horizontal surface.
8 The T-PROGS generated geology above the impermeable clay consists of categorical deposits of sand,
9 silt and clay. Within each of the three types of deposits, hydraulic conductivity, recharge and ~~the~~
10 porosity were generated as horizontally correlated random fields using FIELDGEN (Doherty 2010).
11 All boundaries of the domain were defined as having no-flow conditions except the southern boundary
12 where hydraulic head was defined as constant, $h = 0$ m. The local recharge depends on the type of
13 sediment at the uppermost layer. Most groundwater discharges through the southern boundary, but
14 approximately 35% discharges into a river running- north to south in the middle of the domain (Figure
15 2). Groundwater flow was simulated as confined steady-state flow employing MODFLOW-2000
16 (Harbaugh et al. 2000) with the spatial discretization equal to the geological discretization.
17 Groundwater is pumped at a rate of $0.015 \text{ m}^3\text{s}^{-1}$ from a well located at $x=2487.5\text{m}$ and $y=1912.5 \text{ m}$ and
18 the well screens the deepest 10 meters of the groundwater system. In the following, this system is
19 called the *reference system*.

20 Thirty-five boreholes are found within the domain (Figure 2). Each borehole contains a monitoring
21 well that screens the deepest 10 m of sand registered in the borehole. For each system realization,
22 hydraulic head in the 35 wells and the river discharge at the southern boundary were extracted from a
23 forward simulation made by MODFLOW-2000. The 35 simulated hydraulic head values were
24 contaminated by independent Gaussian error with zero mean and 0.1 m standard deviation. The river
25 discharge was corrupted with independent Gaussian error with zero mean and a standard deviation
26 corresponding to 10-% of the true river discharge. The 36 contaminated values constitute the
27 hydrological data used for groundwater model calibration.

29 **3.2 Geophysical reference system and data**

30 The geophysical reference system was designed so ~~that~~ there is perfect correlation between hydraulic
31 conductivity and electrical resistivity. This implies that a relationship between hydraulic conductivity
32 and measured electrical resistivity is likely to exist. The true relationship is of the same form as eq. ~~(3)~~
33 ~~(3)~~, and it uses constant shape factor values $\alpha = 1e^{-12}$ and $\beta = 4$. This corresponds to conditions

1 where clay has low electrical resistivity and also low hydraulic conductivity, and sand has high
 2 electrical resistivity and high hydraulic conductivity. The impermeable clay at the base of the
 3 reference system was assigned a constant value of 5 ohm-m.

4 The AEM data were simulated using AarhusInv (Auken et al. 2014) for a system setup similar to a
 5 typical dual-moment SkyTEM-304 system (Sørensen and Auken 2004). The simulated survey consists
 6 of 35 E-W flight lines with 200 meter spacing between the flight lines. AEM system responses were
 7 simulated for every 25 m along the flight lines giving a total of 6300 sounding locations for both the
 8 transmitted high and low moments. AarhusInv is a 1D modeling code. To mimic the loss of resolution
 9 with layer depth we simulated the responses using the 2D logarithmic average resistivity of all model
 10 cells inside the radius of the foot print at a given depth. To obtain the geophysical data set, the
 11 simulated data were contaminated with noise according to the noise model suggested by (Auken et al.
 12 2008):

$$V_{resp} = V \cdot \left(1 + G(0,1) \cdot \left[STD^2_{uni} + \left(\frac{V_{noise}}{V} \right)^2 \right]^{1/2} \right) \quad (5)$$

13
 14 where V_{resp} is the perturbed synthetic data, V is the synthetic noiseless data, $G(0,1)$ is standard
 15 Gaussian noise (with zero mean and unit standard deviation), and STD^2_{uni} is uniform noise variance.
 16 V_{noise} is the background noise contribution given by

$$V_{noise} = b \cdot \left(\frac{t}{10^{-3}} \right)^{-1/2}, \quad (6)$$

17
 18 where t is the gate center time in seconds, and b is the background noise level at 1 ms. For the
 19 following analysis we generated geophysical datasets with four levels of background noise, i.e. b equal
 20 to 1, 3, 5, and 10 nV/m², respectively. The uniform standard deviation, which accounts for instrument
 21 and other non-specified noise contributions, was set to 3% for dB/dt responses. After the data were
 22 perturbed with noise, it was processed as a field data set (Auken et al. 2009), resulting in an uneven
 23 number of gates per sounding. [Figure 3](#) illustrates the resulting low and high moment AEM
 24 sounding data, respectively, for the different background noise levels.

25

3.3 Geophysical voxel inversion

The geophysical data were inverted by voxel inversion (Fiandaca et al. 2015) using AarhusInv (Auken et al. 2014). The voxel inversion was conducted in two different ways: by using L2-norm “smooth” constraints, or by using minimum gradient support “sharp” constraints (both implemented in AarhusInv; Auken et al. 2014).

To avoid the influence of numerical discretization errors, the geophysical voxel inversion uses the same spatial discretization as the reference system and the groundwater model. For both smooth and sharp inversions, a 40 ohm-m uniform half-space was used as the starting model, and spatial regularization was applied using the same settings throughout all inversions. Considering the small number of layers and the shallow discretization, it was unnecessary to apply vertical constraints for any of the inversions. ~~On the contrary,~~ depth and direction dependent horizontal constraint factors were used for both smooth and sharp inversions. The strength given to the horizontal constraints is based on experience, keeping in mind that the constraint factors should not prevent data fitting, but must not be too strong preventing fitting the data promote model consistency. Therefore, a few experiments were made to “manually” estimate tune the magnitude of the constraint factors. Furthermore, Different values along the flight lines and perpendicular to them, respectively, were found to give better results. strong inversion artifacts were found in perpendicular to the flight lines when using the same uniform constraint factors along the flight lines as to perpendicular to the flight lines. This is a result of having more higher data density along the flight lines, compared to the perpendicular direction to the flight lines, and that’s why the horizontal contains is different for the two directions. In this these synthetic test case (as in all real cases similarly to what is done with field data with analogous data density) the For smooth regularization constraint factors of 1.9 along the flight lines and 1.05 perpendicular to the flight lines was were used for the first layer.

Contrary to the conventional inversion of geophysical data, Furthermore, where the vertical discretization of the geophysical model is normally characterized by logarithmically increasing layer thicknesses, in this study fixed layer thicknesses were used in the geophysical models. To account for using fixed layer thicknesses in the geophysical model the loss of resolution with depth without increasing the layer thicknesses, the horizontal constrain factors were set to decrease linearly with depth (tighter bands for the deeper layers). The constraint factors was set to decrease linear with depth, resulting in constraint factors of -1.4 along the flight lines and 1.02 perpendicular to the flight lines for the sixth layer.

The conception same directional and depth-dependent tuning used for smooth regularization were as also applied For for to the sharp inversion. In this case constraint factors of 1.0625 along the flight

lines and 1.01 perpendicular to the flight lines ~~was-were~~ used for the first layer, while factors of 1.025 along the flight lines and 1.01 perpendicular to the flight lines ~~was-were~~ used for the sixth layer. The smaller values of the constraint factors in the sharp inversion are due to the different role that the factors play in the regularization definition, as evident when comparing eq. (1) and eq. (2). The difference in constraint values between smooth and sharp inversion is analogous to what has been used in other studies (e.g. Vignoli et al., 2015).

3.4 Groundwater model parametrization and calibration

In the following, the groundwater model will be parameterized in two different ways. Both ways approaches treat the shape factors between hydraulic conductivity and resistivity, α and β , of their relationship (3), ~~between hydraulic conductivity and resistivity~~ as spatially dependent parameters to be estimated. The two parameterizations differ by the resistivity model that is used to calculate the hydraulic conductivity field of the groundwater model:

- The first type of parameterization uses a resistivity model estimated by smooth voxel inversion of AEM data collected with a background noise level of 3 nV/m². These models will be referred to as SHI-smooth-3.
- The second type of parameterization uses a resistivity model estimated by sharp voxel inversion of AEM data collected with a background noise level of either 1, 3, 5, or 10 nV/m². These models will be referred to as SHI-sharp-1, SHI-sharp-3, SHI-sharp-5, and SHI-sharp-10, respectively.

The shape factors, α and β , of the petrophysical relationship are parametrized by placing pilot points in a uniform grid, with 5 nodes in the x direction and 7 in the y direction. Hence, in total the groundwater model is parameterized by $5 \times 7 \times 5 = 175$ petrophysical relationships each having two parameters (the shape factors).

The parameter values are estimated by fitting the available hydrological data consisting of the 35 observations of hydraulic head and one river discharge observation. Calibration is done by minimization the total objective function given by eq. ~~(4)~~(4), where the measurement objective function is computed as

$$\Phi_m = n_h^{-1} \sum_{i=1}^{n_h} \omega_h (h_{obs,i} - h_{sim,i})^2 + n_r^{-1} \sum_{i=1}^{n_r} \omega_r (r_{obs,i} - r_{sim,i})^2 \quad (7)$$

1 where, n_h and n_r are the number of head and river measurements, respectively; h_{obs} and h_{sim} are
2 observed and corresponding simulated hydraulic heads; r_{obs} and r_{sim} are observed and
3 corresponding simulated river discharge; and ω_h and ω_r are subjectively chosen weights for head and
4 discharge data, respectively. If a model is expected not to have structural defects then it would be ideal
5 to choose the weights $\omega_h = \sigma_h^{-1}$ and $\omega_r = \sigma_r^{-1}$, where σ_h and σ_r is the standard deviation of
6 measurement error for head and river measurements, respectively. However, in this case (as in all real
7 cases) the model has structural errors that make the misfit between hydraulic head data and equivalent
8 simulated values much larger than what can be explained by measurement error. In accordance with
9 common groundwater modeling practice (e.g. Christensen et al. 1998), we therefore conducted
10 residual analysis and a few experiments to estimate the magnitude of the total head error (which is the
11 sum of observation error and structural error). This indicated that the standard deviation for the total
12 error on hydraulic head is approximately $10 \cdot \sigma_h$, while the total error for the river discharge is totally
13 dominated by measurement error. As weights we therefore used $\omega_h = (10 \cdot \sigma_h)^{-2} = 1.0$ and
14 $\omega_r = (\sigma_r)^{-2} = 1.38 \cdot 10^5$, respectively. Using these weights, and averaging over the 20 system
15 realizations, gave a minimized objective function value of $\bar{\phi}_m = 2.5$. This is close to the value of 2.0,
16 which would be expected from (7) if the weighting used reflects the error magnitudes.

17 Calibration was performed using ~~local search as optimization implemented in the parameter estimation~~
18 ~~software~~ BeoPEST, a version of PEST (Doherty 2010) that allows the inversion to run in parallel
19 using multiple cores and computers.

20 It should be noted that for calibration and model prediction we applied the recharge field and boundary
21 conditions of the reference system.

22 **3.5 Reference and mModel predictions**

23 In step 3 (Figure 1, box), the calibrated groundwater model is used to make predictions.

24 In the following synthetic demonstration study, the ~~The~~ calibrated SHI-smooth and SHI-sharp
25 groundwater models are evaluated by comparing their simulated model predictions with corresponding
26 predictions simulated for the (synthetic and, therefore, known) reference system. The former are called
27 “model predictions”, the latter are called “reference predictions”.

28 Prediction types 1 and 2 relate to steady-state flow when groundwater is pumped from the well. This is
29 also the condition for which the hydrologic data used for calibration were sampled. Type 1 is the
30 average age of the groundwater pumped from the well. Type 2 is the size of the recharge area of the
31 pumping well. Both of these predictions differ in type from the calibration data. For these model

1 | predictions, we used a homogeneous porosity of 0.2 (the average value of the reference system
2 | porosity fields is 0.184).

3 | Prediction types 3 and 4 relate to a new stress situation long after pumping from the well has ceased:
4 | type 3 is groundwater discharge into the stream, and type 4 is head recovery for a well screening a
5 | layer north-east of the pumping well (the location is shown in on Figure 2).

6 | The reference and model prediction types 3 and 4 were simulated by MODFLOW-2000 (Harbaugh et
7 | al. 2000), while type 1 and 2 were simulated by forward particle tracking using MODPATH version 5
8 | (Pollock 1994) and MODFLOW-2000 results.

9 | The first two types of prediction are interesting from the perspectives of protection and resource-
10 | management of a well field, while the latter two are relevant in the case of possible change of
11 | management practice resulting in a new stress.

12

13 | 3.6 Evaluation of prediction performance

14 | As said in the beginning of section 2, steps 1-3 of the framework can be repeated for a number of
15 | system realizations to provide for making consistent statistical inference on regarding the model
16 | prediction results. Here, 20 different reference system realizations were used. For each prediction, we
17 | therefore hereby have 20 corresponding sets of reference predictions and model predictions that can be
18 | used to evaluate the performance of a calibrated model with respect to that prediction. The
19 | performance is evaluated for SHI-smooth and SHI-sharp models, respectively, and it is done in the
20 | following ways.

21 | Prediction error characteristics are quantified by the mean absolute error (*MAE*), the mean error (*ME*)
22 | following, respectively:

23

$$MAE = \frac{1}{N} \sum_{i=1}^N |x_i - t_i| \quad (8)$$

$$ME = \frac{1}{N} \sum_{i=1}^N x_i - t_i \quad (9)$$

24

25 | where x_i is the model prediction of realization i , t_i is the reference prediction of realization i , and
26 | $N = 20$ is the number of system realizations. *MAE* measures how close the model prediction tends to

1 be to the reference prediction; *ME* measures the tendency of positive or negative bias in the model
2 prediction.

3

4 **4 Results**

5 **4.1 Geophysical results**

6 ~~Figure 4~~ shows a representative cross-section for one of the 20 system realizations. Both
7 geophysical models in ~~Figure 4~~ were inverted using data perturbed with a background noise
8 level of 3nV/m^2 . Comparing the geophysical model results with the reference model, we find that the
9 SHI-smooth-3 resolves the main features reasonably well for the upper layers. The main discrepancy
10 is found in the fifth layer, where the sand bodies are not resolved. In general, the resistivity of the
11 sand bodies (dark orange in the reference system) is underestimated, and the transitions between the
12 categorical deposits are artificially smooth.

13 ~~Figure 4~~ shows that SHI-sharp-3 resolves the sand body in layer 5 much better than SHI-
14 smooth-3. Moreover, the locations and boundaries of the geological deposits tend to be less smeared
15 out when using the sharp constraints. Inspection of the histograms at the bottom of ~~Figure 4~~
16 shows that the SHI-sharp-3 model tends to produce resistivity distributions that ~~are~~ have more
17 similarities with to the reference distributions than the SHI-smooth-3 model. This improvement ~~should~~
18 could potentially allow for easier translation from electrical resistivity into hydraulic conductivity and
19 correspondingly more faithful representation of hydrogeologic structure and connectivity.

20 Figure 5 shows ~~corresponding~~ voxel by voxel density plots of reference versus estimated electrical
21 resistivity for a SHI-smooth model and corresponding SHI-sharp models. Pearson's correlation
22 coefficient (PCC; Cooley and Naff 1990) is shown on top of the density plot for each layer. A
23 comparison of the density plots and the PCC values of the SHI-smooth-3 and SHI-sharp-3 models
24 shows that using sharp instead of smooth constraints improves the inverted geophysical model. The
25 improvement is seen most clearly ~~seen~~ for the sand deposits

26 For both SHI-smooth and SHI-sharp models there is a strong correlation between the electrical
27 resistivity estimates and the true electrical resistivities of the first layer, but the SHI-smooth model has
28 weaker correlation than the SHI-sharp models. For both types of models, the correlation weakens with
29 depth and background noise. The former is caused by the resolution limitations of AEM data.
30 However, the depth and resistivity of the low-resistivity clay at the base of the model are well resolved
31 by both the SHI-smooth and SHI-sharp models inversions (results not shown).

4.2 Hydrological calibration results

The calibration results for the 20 different system realizations are shown in ~~Figure 6~~~~Figure-6~~. The figure shows ~~that~~ the measurement objective function value, Φ_m , for ~~each-most~~ system realizations ~~is~~ close 2.0. ~~We aimed at using weights that would make the minimized measurement objective function value averaged over the 20 system realizations approximately equal to 2. Figure 6 shows that this is nearly satisfied by~~ This is the case for almost all of the ~~the~~ SHI-Sharp model ~~realizations~~, ~~and~~ even for large background noise levels. For many of the realizations, the SHI-Smooth model also fits the data well, but, ~~several for a couple of~~ realizations ~~lead to higher the~~ misfit ~~is much larger than aimed at than~~ ~~desired~~. This makes $E[\Phi_m]$ equal to 5.8 for SHI-Smooth-3 models while it is 2.5 for the SHI-Sharp-3 models. ~~That is, This indicates that~~ the estimated hydraulic conductivity field tends to be ~~better less~~ ~~wrong~~ for sharp models than for smooth models.

4.3 Parameter estimation

~~Figure 7~~~~Figure-7~~ shows a cross section of the estimated K -, α - and β - fields for one of the system realizations. The two columns show estimates for the SHI-smooth-3 and SHI-sharp-3 models, ~~respectively~~. ~~Figure 8~~~~Figure-8~~ shows a density plot of the reference hydraulic conductivity distribution and the estimated hydraulic conductivity distributions. The results in ~~Figure 7~~~~Figure-7~~ and ~~Figure 8~~~~Figure-8~~ are typical for all 20 system realizations.

From ~~Figure 7~~~~Figure-7~~ a) and ~~Figure 7~~~~Figure-7~~ b) it is seen that the estimated α and β parameter values ~~are changing change~~ smoothly in the horizontal direction but have sharp transitions in the vertical direction. The second row of ~~Figure 7~~~~Figure-7~~ shows the corresponding estimated K fields whose main features are determined by the underlying resistivity models (~~Figure 4~~~~Figure-4~~), but they are “corrected” during model calibration to make the groundwater ~~model~~ fit the hydrological data.

For the SHI-smooth-3 model, α and β are taking compensatory roles particularly in the first layer. Here, the estimated α and β values ~~in this layer~~ are higher than the shape factors of the true relationship that was used to construct the geophysical reference system. This increases the hydraulic conductivity in layer 1 to compensate for the too low hydraulic conductivity (and resistivity, ~~Figure 4~~~~Figure-4~~) in layer 2 and deeper layers. The estimated α and β values are not sufficient to compensate for the missing deep high-resistivity body in in layer 5 of the SHI-Smooth-3 model (~~Figure 4~~~~Figure-4~~).

For the SHI-sharp-3 model, the estimated α and β parameter values only vary slightly from the shape factor values of the true relationship except for layer 5 (~~Figure 7~~~~Figure-7~~ b)). This indicates that for the

1 | ~~more-shallow~~er layers the sharp inversion of AEM data sufficiently resolves the resistivity of features
2 | that are important for groundwater model calibration. In layer 5 the estimate of shape factor β turns
3 | out to be fairly high; ~~this-to~~compensates for the too low resistivity estimates in this layer (~~Figure~~
4 | ~~4~~Figure-4).

5 | ~~Figure 8~~Figure-8 shows voxel by voxel density plots of reference versus estimated hydraulic
6 | conductivity for SHI-smooth and SHI-sharp models. ~~The figure is equivalent to Figure 5. Figure 8~~The
7 | results confirms that the ~~resulting~~K field tends to be overestimated for the first layer, ~~and~~in particular
8 | for the SHI-smooth-3 model. From the second layer and ~~deeper,~~own the hydraulic conductivity values
9 | tend to be underestimated for sand but overestimated for silt and clay. Moreover, the distributions of
10 | estimated K smear out with depth. Judged by PCC values and visual inspection of ~~Figure 8~~Figure-8
11 | (highlighting connectivity of the K field), the hydraulic conductivity field estimated for ~~any~~SHI-sharp
12 | ~~models~~ is in better agreement with the reference field than the field estimated by the SHI-Smooth-3
13 | model.

14 | Model structural accuracy is quantified in

1 | ~~Table 1~~ for both the SHI-smooth and SHI-sharp models. Structural accuracy is ~~here~~-calculated ~~here~~ as
2 | the fraction of total number of voxels for which the estimated \log_{10} -hydraulic conductivity plus/minus twenty
3 | percent contains the true \log_{10} -hydraulic conductivity value of the reference model. The results are averaged
4 | over the 20 system realizations. From

1 ~~Table 1~~ it is seen that all SHI-sharp models outperform the accuracy of the SHI-smooth models
2 except for layer 5. The exception occurs because the SHI-smooth models are fairly good at estimating
3 the K distributions for silt and clays, but underestimates K for sand (~~Figure 8~~). On the
4 contrary, SHI-sharp models overestimate the K distributions for silt and clays, but only slightly
5 underestimate K for sand (~~Figure 8~~). Therefore, for layer 5, the model structural accuracy
6 appears to be better for SHI-smooth than for SHI-sharp models.

8 4.4 Prediction results

9 For each of the 20 system realizations, the calibrated groundwater models were used to make the
10 model predictions described in section 3.5. ~~Figure 9~~ shows scatter plots of reference
11 prediction versus the calibrated model prediction; each plotted point corresponds to a particular system
12 realization and corresponding SHI-smooth-3 or SHI-sharp-3 model. The mean error (ME) and mean
13 absolute error (MAE) of the prediction are also given in ~~Figure 9~~. ~~Figure 10~~ shows a
14 MAE contour map for head recovery predictions.

16 4.4.1 Particle tracking predictions

17 The first column of ~~Figure 9~~ shows results for prediction of average age of the groundwater
18 pumped from the pumping well. The scatter plot illustrates that SHI-sharp models tend to over-predict
19 average age. This is seen by the majority of points plotting above the identity line as well as by the
20 value of $ME = 32$ (~~Figure 9~~). The age prediction results are similar for the SHI-smooth models
21 although the spread of points is larger than for SHI-sharp-3 (e.g. quantified by the larger value of
22 MAE). There are two major explanations for these relatively “poor” predictive performances. First, the
23 calibrated K -fields underestimate hydraulic conductivity of sand deposits in the deeper layers (~~Figure~~
24 ~~8~~), which results in too slow particle travel times at depth. Secondly, the reconstruction of the
25 deepest layers is too smooth for both SHI-smooth and SHI-sharp models (~~Figure 7~~) and does
26 not resolve the small-scale variability that controls the transport of particles.

27 The second column of ~~Figure 9~~ reports results related to prediction of the recharge area
28 of the pumping well. The scatter plot shows that the SHI-smooth models under-predicts the recharge
29 area. This happens because the smooth models lead to estimation of hydraulic conductivities in the
30 deepest layers that are too low. This creates a deep cone of depression around the pumping well that
31 extends upward locally to reach the river bed. This induces a local discharge of water from the stream
32 through the groundwater system to the pumping well. These models thus predict that a significant

1 proportion of the pumping comes from local discharge from the river. (This is compensated by
2 increased model predicted groundwater discharge to other parts of the river.) ~~For the true, reference~~
3 ~~system used to generate the data~~ ~~For the corresponding reference systems~~, the river is not losing water,
4 and all water pumped from the well originates from groundwater recharge.

5 The SHI-sharp models are better predictors of the recharge area, but also these models tend to predict
6 an area that is too small. These models also predict local discharge from the river to the groundwater
7 system, but to a lesser degree than the SHI-smooth models. This is likely because the main features of
8 the reference system are better reconstructed by the SHI-sharp-3 models.

9

10 4.4.2 Head recovery and discharge predictions

11 The prediction of head recovery at ~~the an~~ observation well (location shown in Figure 10) is done
12 poorly by the SHI-smooth-3 (~~Figure 9~~ ~~Figure 9~~). The predicted head recovery is very small for most of
13 these models because they tend to have too little hydraulic connectivity between the deepest layers, the
14 estimated hydraulic conductivities are too low in the deep sand layers, and the simulated cone of
15 depression is therefore too deep and too local.

16 The SHI-sharp-3 models make less biased, fairly reasonable predictions of the head recovery (~~Figure~~
17 ~~9~~ ~~Figure 9~~) because they resolve the variations of hydraulic conductivity at depth better than the SHI-
18 smooth-3 models. The superiority of ~~SHI-smooth~~ ~~sharp~~-3 models for recovery prediction is also seen
19 from the *MAE* contour maps in ~~Figure 9~~ ~~Figure 9~~. The *MAE* is seen to be spatially dependent: it is
20 largest at the pumping well, and smallest at the constant head boundary to the south

21 The fourth column of ~~Figure 9~~ ~~Figure 9~~ shows that both types of models are good predictors of
22 discharge to the river after cessation of pumping. However, the SHI-sharp-3 model prediction is
23 superior (~~since~~ ~~its points~~ ~~tend to~~ ~~plot closer~~ to the identity line). For SHI-smooth-3, the prediction
24 tends to be positively biased and more spread than for SHI-sharp-3.

25

26 4.4.3 Prediction error as function of data quality

27 In ~~Figure 11~~ ~~Figure 11~~ *MAE* is used as a metric to evaluate how the prediction performance of SHI-
28 sharp models depends on the level of background noise for the geophysical data. The noise levels were
29 kept unchanged for the hydrological data.

30 ~~Figure 11~~ ~~Figure 11~~ shows that the average age prediction made by SHI-sharp models are nearly
31 unaffected by the quality of the geophysical data. It is speculative, but this result may be because this

1 prediction is highly ~~dependable~~ dependent on small scale variability in hydraulic conductivity and
2 porosity that cannot be resolved from any of the geophysical data sets. That is, even the highest
3 quality geophysical data are not highly informative, so reducing the data quality further has little
4 effect.

5 It is different for the recharge area prediction (~~Figure 11~~ Figure 11): MAE increases for this by
6 approximately 25% when the level of background noise is increased from 1 nV/m² to 10 nV/m². This
7 happens because the variations of resistivity (and thus hydraulic conductivity) are less well resolved
8 when using the poor quality ~~from the~~ geophysical data ~~of poor quality~~.

9 The third and fourth rows of ~~Figure 11~~ Figure 11 shows the head recovery and river discharge
10 prediction after cessation of the pumping well. Head recovery and discharge predictions also tend to
11 depend on the quality of the geophysical data. The MAE increases by 17 % for recovery prediction and
12 23 % for discharge prediction when the noise level of the geophysical data increases from 1 nV/m² to
13 10 nV/m².

14

1 5 Discussion

2 5.1 Estimation of Parameters in the Petrophysical Relation

3 Parameterizing the groundwater model by assuming a spatially dependent petrophysical relationship
4 between resistivity and hydraulic conductivity makes it possible to use a resistivity voxel model for
5 construction and calibration of a groundwater model. ~~By a~~ Assuming that the relationship ~~to be~~ is
6 spatially dependent can account for two challenges: i) there may be actual changes in the petrophysical
7 relationship within an investigated domain, and ii) there may be resolution limitations in the estimated
8 resistivity model.

9 Challenge i) is likely to be the rule for many environments, especially can for example be expected for
10 sedimentary environments, where the formation resistivity is primarily controlled by the pore water
11 resistivity and the clay content. In the case of spatially changes of pore water resistivity and/or content
12 of various clay minerals content, the discrimination between clay and sands may be less clear in the
13 estimated resistivity values. For large-scale groundwater system, the variation of pore water resistivity
14 (e.g. saline pore water) is expected to vary smoothly, which would be accounted for by the spatially
15 varying petrophysical relationship. However, the procedure only works as applied here if the
16 underlying assumption is valid, that clay rich deposits have lower electrical resistivity compared to
17 than sands deposits is valid, is valid.

18 Challenge ii) concerns the geophysical model resolution of the true formation resistivity. EM methods
19 are, by nature, more sensitive to deposits of low electrical resistivity than to deposits of high
20 resistivity, and their vertical and horizontal resolutions decrease with depth. This challenge is what
21 affects the resistivity models estimated in the present synthetic study. ~~Estimating s~~ Spatially dependent
22 shape factors ~~by groundwater model calibration let allow them can~~ take a compensatory role for the
23 resolution issues of the estimated geophysical voxel model. The calibrated shape factors may thus no
24 longer have firm physical meaning since because they mainly act as correction parameters for
25 absorbing structural errors of the geophysical model. ~~T,~~ The estimation of locally unreasonable
26 shape factors may be this is acceptable as long as the resulting hydraulic conductivity values are
27 reasonable. The idea of calibrating the shape factors is related to the concept of compensatory
28 parameters in highly parameterized calibration described by Doherty and Welter (2010) and by
29 Doherty and Christensen (2011).

30 Finally, Auken et al. (2008) showed that using borehole data as a priori information in the geophysical
31 inversion improves the reconstruction of the model features significantly. Estimation of EM-based
32 resistivity models should therefore, in general wherever possible, be supported ~~by~~ borehole
33 information to improve the decreasing spatial resolution of the EM methods.

1

2 | 5.2 Geophysical inversion strategy and ~~d~~Data quality

3 | Inversion of AEM data using a 1D geophysical model usually applies smoothness constraints in order
4 | to regularize the inversion (Auken and Christiansen 2004; Viezzoli et al. 2008). Traditionally, the
5 | regularization includes both lateral and vertical smoothing constraints (Constable et al. 1987) or a few
6 | layer parametrization (Auken et al. 2008). Inversion using the former type of regularization produces
7 | smooth images with blurred formation boundaries which can be problematic when it is important to
8 | resolve structural connections in a complex geological system. The latter few-layer inversion may is
9 | also be prone to produce artifacts when used to map ~~complex geological environments such systems. It~~
10 | ~~has therefore been recognized, e.g. by~~ Day-Lewis (2005) and others ~~therefore recognized,~~ that ~~the~~
11 | regularization used to stabilize the geophysical inversion ~~may can~~ lead to artifacts that do not reflect
12 | the actual hydrogeological conditions. Thoughtless use of such results to construct groundwater
13 | models ~~for making hydrologic predictions~~ can ~~therefore~~ have serious ramifications.

14

15 | ~~Furthermore,~~ for the present case study, the number of vertical transitions is a great challenge for the
16 | AEM method due to the principle of high resistivity equivalence. ~~T:~~ that is, it is difficult to resolve a
17 | high-resistivity layer between two low-resistivity layers because the energy loss, and therefore the
18 | sensitivity, is concentrated in the ~~more-less~~ resistive layers. This will result in layer suppression,
19 | because the data sensitivity to the high resistive layer is low (Christiansen et al. 2006). This effect is
20 | present for both the smooth and sharp inversion, but in the sharp inversion the effect is less fuzzy and
21 | features, especially for the fifth layer, ~~are could be~~ more clearly reconstructed (~~Figure 4~~~~Figure-4~~).
22 | When the sensitivity of the AEM method is too low, the ~~contribution from the~~ regularization may
23 | ~~make dominate, and~~ information ~~might~~ migrate from areas with higher measurement sensitivity
24 | (Vignoli et al. 2015). In contrast to the smooth regularization scheme, the sharp regularization method
25 | is designed to penalize smooth transitions, which eventually improves the reconstruction of the deeper
26 | sand bodies ~~in the present study~~. Therefore, for the ~~present studied~~ case-~~study~~ the sharp regularization
27 | methodology should be preferred over smooth regularization, because ~~the~~ sharp constraints correspond
28 | better to the ~~true-actual-~~ structures of the reference system (~~eategorical deposits with~~ sharp transitions
29 | ~~between categorical deposits~~; ~~Figure 4~~~~Figure-4~~). Moreover, because the sharp regularization
30 | methodology leads to improved reconstruction of subsurface structures, these models lead to greater
31 | accuracy and improvement of most groundwater model predictions (~~Figure 9~~~~Figure-9~~).

32

33 | The groundwater system considered here is relatively shallow, at least ~~as~~ seen from the perspective of
34 | the AEM system used in the demonstration example. This is evident from the transmitted EM signal

1 (~~Figure 3~~~~Figure-3~~). The background noise is primarily affecting the last time-gates (10^{-4} - 10^{-3} s) of the
2 low-moment and only ~~£~~to a small degree the high moment time gates (even for low quality data). This
3 implies that the resolution of the AEM data is generally high for the upper layers. Therefore, in the
4 present case the upper layers of all the geophysical models (both SHI-smooth and SHI-sharp) are well-
5 resolved and to a large extent unaffected by AEM data quality (~~Figure 5~~~~Figure-5~~). However, the deep
6 sand units are difficult to resolve because they give only a weak signature in the AEM data (~~Figure~~
7 ~~3~~~~Figure-3~~, ~~Figure 5~~~~Figure-5~~). This is particularly true for the poorest AEM data quality cases where
8 the late time gates for the low moment measurements are disturbed by background noise.

9 **6 Summary and Conclusion**

10 We present a workflow for ~~automated-efficient~~ construction and calibration of large-scale groundwater
11 models using a combination of airborne electromagnetic (AEM) data and hydrological data, ~~but~~
12 ~~e~~Other types of data could be integrated as well ~~following the same procedure~~. First, the AEM data are
13 inverted to form a 3D geophysical model. Subsequently, the geophysical model is translated to a 3D
14 model of hydraulic conductivity by using a spatially dependent petrophysical relationship for which
15 the shape parameters are estimated by fitting the groundwater model to hydrological data. The
16 estimated shape factors of the petrophysical relationship primarily work as translators between
17 resistivity and hydraulic conductivity, but they can also compensate for structural defects in the model.

18 The method is demonstrated for a synthetic case study where the subsurface consists of categorical
19 deposits with different geophysical and hydraulic properties. The AEM data are inverted using both
20 smooth and sharp regularization constraints, resulting in two competitive geophysical models.
21 Furthermore, the influence of the AEM data quality is tested by inverting the sharp geophysical
22 models using data corrupted with four different levels of background noise. The resulting groundwater
23 models are each calibrated on basis of head and discharge data, and their predictive performance is
24 tested for four types of prediction beyond the calibration base. Predictions of a pumping well's
25 recharge area and groundwater age are applying the same stress situation as applied during hydrologic
26 model calibration, while predictions of head and stream discharge is done for a changed stress
27 situation.

28 It is found that a geophysical model inverted with sharp constraints (SHI-sharp) leads to a more
29 accurate groundwater model than one that is based on a geophysical model inverted with smooth
30 constraints (SHI-smooth). The SHI-sharp model leads to an estimated hydraulic conductivity field of
31 greater accuracy and to improvement of most groundwater model predictions. The explanation is that
32 the reference system (like many real hydrogeologic systems) is characterized by sharp transitions

1 | between ~~the~~ categorical deposits; this is resolved better by the SHI-sharp resistivity model than by the
2 | SHI-smooth model.

3 | Finally, it is shown that prediction accuracy improves with AEM data quality for predictions of
4 | recharge area, head change and stream discharge, while the accuracy appears to be unaffected ~~not~~
5 | improve for prediction of groundwater age, which cannot be predicted accurately even with high
6 | quality geophysical data.

1 7 References

- 2 Abraham JD, Cannia JC, Bedrosian PA, Johnson MR, Ball LB, Sibray SS (2012) : Airborne
3 Electromagnetic Mapping of the Base of Aquifer in Areas of Western Nebraska. In: U.S. Geol.
4 Surv. Sci. Investig. Rep. 2011–5219. <http://pubs.usgs.gov/sir/2011/5219/>. Accessed 4 Jan 2016
- 5 Archie GE (1942) : The Electrical Resistivity Log as an Aid in Determining Some Reservoir
6 Characteristics. *Trans AIME* 146:54–62. doi: 10.2118/942054-G
- 7 Auken E, Christiansen A V., Jacobsen LH, Sørensen KI (2008) : A resolution study of buried valleys
8 using laterally constrained inversion of TEM data. *J Appl Geophys* 65:10–20.
- 9 Auken E, Christiansen AV (2004) : Layered and laterally constrained 2D inversion of resistivity data.
10 *GEOPHYSICS* 69:752–761. doi: 10.1190/1.1759461
- 11 Auken E, Christiansen AV, H.Westergaard J, Kirkegaard C, Foged N, Viezzoli A (2009) : An
12 integrated processing scheme for high-resolution airborne electromagnetic surveys, the SkyTEM
13 system. *Explor Geophys* 40(2):184–192. doi: <http://dx.doi.org/10.1071/EG08128>
- 14 Auken E, Christiansen AV, Kirkegaard C, Fiandaca G, Schamper C, Behroozmand AA, Binley A,
15 Nielsen E, Effersø F, Christensen NB, Sørensen K, Foged N, Vignoli G (2014) : An overview of
16 a highly versatile forward and stable inverse algorithm for airborne, ground-based and borehole
17 electromagnetic and electric data. *Explor Geophys* 46(3):223–235. doi: 10.1071/EG13097
- 18 Bedrosian PA, Schamper C, Auken E (2015) : A comparison of helicopter-borne electromagnetic
19 systems for hydrogeologic studies. *Geophys Prospect* 64:192–215. doi: 10.1111/1365-
20 2478.12262
- 21 Binley A, Hubbard SS, Huisman JA, Reil A, Robinson DA, Singha K, Slater LD (2015) : The
22 emergence of hydrogeophysics for improved understanding of subsurface processes over
23 multiple scales. *Water Resour Res* 51:3837–3866. doi: 10.1002/2015WR017016
- 24 Blaschek R, Hördt A, Kemna A (2008) : A new sensitivity-controlled focusing regularization scheme
25 for the inversion of induced polarization data based on the minimum gradient support.
26 *GEOPHYSICS* 73:F45–F54. doi: 10.1190/1.2824820
- 27 Carle SF (1999) T-PROGS: Transition Probability Geostatistical Software. Users Manual. Version
28 2.1. University of California, Davis
- 29 Carle SF, Fogg GE (1996) : Transition probability-based indicator geostatistics. *Math Geol* 28:453–
30 476. doi: 10.1007/BF02083656
- 31 Certes C, De Marsily G (1991) : Application of the pilot point method to the identification of aquifer
32 transmissivities. *Adv Water Resour* 14:284–300. doi: 10.1016/0309-1708(91)90040-U
- 33 Chen J, Hubbard S, Rubin Y (2001) : Estimating the hydraulic conductivity at the south oyster site
34 from geophysical tomographic data using Bayesian Techniques based on the normal linear
35 regression model. *Water Resour Res* 37:1603–1613. doi: 10.1029/2000WR900392
- 36 Christensen NK, Christensen S, Ferre TPA (2016) : Testing alternative uses of electromagnetic data to
37 reduce the prediction error of groundwater models. *Hydrol Earth Syst Sci* 20:1925–1946. doi:
38 10.5194/hess-20-1925-2016
- 39 Christensen S, Rasmussen KR, Moller K (1998) : Prediction of Regional Ground Water Flow to
40 Streams. *Ground Water* 36:351–360. doi: 10.1111/j.1745-6584.1998.tb01100.x

- 1 Christiansen A V., Auken E, Sørensen K (2006) : The transient electromagnetic method. In: Kirsch R
2 (ed) Groundwater Geophysics - A tool for hydrogeology, first ed. Springer-Verlag,
3 Berlin/Heidelberg, pp 179–225
- 4 Christiansen AV, Auken E, Viezzoli A (2011) : Quantification of modeling errors in airborne TEM
5 caused by inaccurate system description.
- 6 Clavier C, Coates G, Dumanoir J (1984) : Theoretical and Experimental Bases for the Dual-Water
7 Model for Interpretation of Shaly Sands. Soc Pet Eng J 24:153–168. doi: 10.2118/6859-PA
- 8 Constable SC, Parker RL, Constable CG (1987) : Occam's inversion: A practical algorithm for
9 generating smooth models from electromagnetic sounding data. GEOPHYSICS 52:289–300. doi:
10 10.1190/1.1442303
- 11 Cooley RL, Naff RL (1990) : Regression modeling of ground-water flow.
- 12 Day-Lewis FD (2005) : Applying petrophysical models to radar travel time and electrical resistivity
13 tomograms: Resolution-dependent limitations. J Geophys Res 110:B08206. doi:
14 10.1029/2004JB003569
- 15 Desbarats AJ, Srivastava RM (1991) : Geostatistical characterization of groundwater flow parameters
16 in a simulated aquifer. Water Resour Res 27:687–698. doi: 10.1029/90WR02705
- 17 Deutsch C V. (2006) : A sequential indicator simulation program for categorical variables with point
18 and block data: BlockSIS. Comput Geosci 32:1669–1681. doi: 10.1016/j.cageo.2006.03.005
- 19 Deutsch C V., Journel AG (1998) GSLIB: Geostatistical Software Library and User's Guide: Clayton
20 V. - Oxford University Press, Second Edi. Oxford University Press
- 21 Doherty J (2003) : Ground Water Model Calibration Using Pilot Points and Regularization. Ground
22 Water 41:170–177. doi: 10.1111/j.1745-6584.2003.tb02580.x
- 23 Doherty J (2010) PEST, Model-Independent Parameter Estimation, User Manual, 5th ed, 336 pp.,
24 Watermark Numerical Computing
- 25 Doherty J, Christensen S (2011) : Use of paired simple and complex models to reduce predictive bias
26 and quantify uncertainty. Water Resour Res 47(12):W12534. doi: 10.1029/2011WR010763
- 27 Doherty J, Welter D (2010) : A short exploration of structural noise. Water Resour Res 46
28 (5):W05525. doi: 10.1029/2009WR008377
- 29 Ferré T, Bentley L, Binley A, Linde N, Kemna A, Singha K, Holliger K, Huisman JA, Minsley B
30 (2009) : Critical Steps for the Continuing Advancement of Hydrogeophysics. Eos, Trans Am
31 Geophys Union 90:200. doi: 10.1029/2009EO230004
- 32 Fiandaca G, Kirkegaard C, Foged N, Christiansen AV, Auken E (2015) : Sharp Spatially-decoupled
33 Inversion of Airborne Electromagnetic Data for Improved Model Integration. In: First European
34 Airborne Electromagnetics Conference.
- 35 Fogg GE, LaBolle EM, Weissmann GS (1999) Groundwater Vulnerability Assessment:
36 Hydrogeologic Perspective and Example from Salinas Valley, California. American Geophysical
37 Union, Washington, D. C.
- 38 Gunnink JL, Siemon B (2015) : Applying airborne electromagnetics in 3D stochastic geohydrological
39 modelling for determining groundwater protection. Near Surf Geophys 13:45–60. doi:
40 10.3997/1873-0604.2014044

- 1 Harbaugh AW, Banta ER, Hill MC, McDonald MG (2000) MODFLOW-2000, The U.S. Geological
2 Survey modular ground-water model: User guide to modularization concepts and the ground-
3 water flow process. U.S. Geological Survey Open-File Report 00-92, 121 p.
- 4 He X, Koch J, Sonnenborg TO, Jørgensen F, Schamper C, Christian Refsgaard J (2014) : Transition
5 probability-based stochastic geological modeling using airborne geophysical data and borehole
6 data. *Water Resour Res* 50:3147–3169. doi: 10.1002/2013WR014593
- 7 Herckenrath D, Fiandaca G, Auken E, Bauer-Gottwein P (2013) : Sequential and joint
8 hydrogeophysical inversion using a field-scale groundwater model with ERT and TDEM data.
9 *Hydrol Earth Syst Sci* 17:4043–4060. doi: 10.5194/hess-17-4043-2013
- 10 Hill M (1998) : Methods and guidelines for effective model calibration; with application to UCODE, a
11 computer code for universal inverse modeling, and MODFLOWP, a computer code for inverse
12 modeling with MODFLOW. *Water-Resources Investig Rep* 98-4005. doi:
13 10.1061/40517(2000)18
- 14 Hyndman D., Tronicke J (2005) : Hydrogeophysical case studies at the local scale: the saturated zone.
15 In: Rubin Y, Hubbard SS (eds) *Hydrogeophysics*. Springer Netherlands, Dordrecht, pp 391–412
- 16 Jørgensen F, Lykke-Andersen H, Sandersen PBE, Auken E, Nørmark E (2003) : Geophysical
17 investigations of buried Quaternary valleys in Denmark: an integrated application of transient
18 electromagnetic soundings, reflection seismic surveys and exploratory drillings. *J Appl Geophys*
19 53:215–228.
- 20 Jørgensen F, Møller RR, Nebel L, Jensen N-P, Christiansen AV, Sandersen PBE (2013) : A method
21 for cognitive 3D geological voxel modelling of AEM data. *Bull Eng Geol Environ* 72:421–432.
22 doi: 10.1007/s10064-013-0487-2
- 23 Linde N, Finsterle S, Hubbard S (2006) : Inversion of tracer test data using tomographic constraints.
24 *Water Resour Res*. doi: 10.1029/2004WR003806
- 25 Marker PA, Foged N, He X, Christiansen A V., Refsgaard JC, Auken E, Bauer-Gottwein P (2015) :
26 Performance evaluation of groundwater model hydrostratigraphy from airborne electromagnetic
27 data and lithological borehole logs. *Hydrol Earth Syst Sci* 19:3875–3890. doi: 10.5194/hess-19-
28 3875-2015
- 29 Mazáč O, Kelly WE, Landa I (1985) : A hydrogeophysical model for relations between electrical and
30 hydraulic properties of aquifers. *J Hydrol* 79:1–19.
- 31 McNeill JD (1980) : *Electromagnetic Terrain Conductivity Measurement at Low Induction Numbers*,
32 Tech. Note TN-6.
- 33 Menke W (2012) *Geophysical Data Analysis: Discrete Inverse Theory, Third Edition: MATLAB*
34 *Edition*. Elsevier, Academic Press, Boston, USA.
- 35 Munday T, Gilfedder M, Taylor Andrew r, Ibrahimi T, Ley-cooper Y, Cahill K, Smith S, Costar A
36 (2015) : The role of airborne geophysics in facilitating long-term outback water solutions to
37 support mining in South Australia. *Water - J Aust Water Assoc* 42:138–141.
- 38 Oldenborger GA, Pugin AJ-M, Pullan SE (2013) : Airborne time-domain electromagnetics, electrical
39 resistivity and seismic reflection for regional three-dimensional mapping and characterization of
40 the Spiritwood Valley Aquifer, Manitoba, Canada. *Near Surf Geophys* 11:63–74. doi:
41 10.3997/1873-0604.2012023
- 42 Pollock DW (1994) *User 's Guide for MODPATH / MODPATH-PLOT , Version 3 : A particle*

- 1 tracking post-processing package for MODFLOW , the U . S . Geological Survey finite-
2 difference ground-water flow model.
- 3 Portniaguine O, Zhdanov MS (1999) : Focusing geophysical inversion images. *GEOPHYSICS*
4 64:874–887. doi: 10.1190/1.1444596
- 5 Refsgaard JC, Christensen S, Sonnenborg TO, Seifert D, Højberg AL, Troldborg L (2012) : Review of
6 strategies for handling geological uncertainty in groundwater flow and transport modeling. *Adv*
7 *Water Resour* 36:36–50. doi: 10.1016/j.advwatres.2011.04.006
- 8 Revil A, Cathles LM (1999) : Permeability of shaly sands. *Water Resour Res* 35:651–662. doi:
9 10.1029/98WR02700
- 10 Revil A, Karaoulis M, Johnson T, Kemna A (2012) : Review: Some low-frequency electrical methods
11 for subsurface characterization and monitoring in hydrogeology. *Hydrogeol J* 20:617–658. doi:
12 10.1007/s10040-011-0819-x
- 13 Robinson DA, Binley A, Crook N, Day-Lewis FD, Ferré TPA, Grauch VJS, Knight R, Knoll M,
14 Lakshmi V, Miller R, Nyquist J, Pellerin L, Singha K, Slater L (2008) : Advancing process-based
15 watershed hydrological research using near-surface geophysics: a vision for, and review of,
16 electrical and magnetic geophysical methods. *Hydrol Process* 22:3604–3635. doi:
17 10.1002/hyp.6963
- 18 Schamper C, Jørgensen F, Auken E, Effersø F (2014) : Assessment of near-surface mapping
19 capabilities by airborne transient electromagnetic data — An extensive comparison to
20 conventional borehole data. *GEOPHYSICS* 79:B187–B199. doi: 10.1190/geo2013-0256.1
- 21 Seifert D, Sonnenborg TO, Refsgaard JC, Højberg AL, Troldborg L (2012) : Assessment of
22 hydrological model predictive ability given multiple conceptual geological models. *Water*
23 *Resour Res* 48:W06503. doi: 10.1029/2011WR011149
- 24 Siemon B, Christiansen AV, Auken E (2009) : A review of helicopter-borne electromagnetic methods
25 for groundwater exploration. *Near Surf Geophys* 7:629–646. doi: 10.3997/1873-0604.2009043
- 26 Slater L (2007) : Near Surface Electrical Characterization of Hydraulic Conductivity: From
27 Petrophysical Properties to Aquifer Geometries—A Review. *Surv Geophys* 28:169–197. doi:
28 10.1007/s10712-007-9022-y
- 29 Strebelle S (2002) : Conditional Simulation of Complex Geological Structures Using Multiple-Point
30 Statistics. *Math Geol* 34:1–21. doi: 10.1023/A:1014009426274
- 31 Sørensen KI, Auken E (2004) : SkyTEM – a new high-resolution helicopter transient electromagnetic
32 system. *Explor Geophys* 35:194–202.
- 33 Thomsen R, Søndergaard VH, Sørensen KI (2004) : Hydrogeological mapping as a basis for
34 establishing site-specific groundwater protection zones in Denmark. *Hydrogeol J* 12:550–562.
35 doi: 10.1007/s10040-004-0345-1
- 36 Viezzoli A, Christiansen AV, Auken E, Sørensen K (2008) : Quasi-3D modeling of airborne TEM
37 data by spatially constrained inversion. *GEOPHYSICS* 73:F105–F113. doi: 10.1190/1.2895521
- 38 Vignoli G, Fiandaca G, Christiansen AV, Kirkegaard C, Auken E (2015) : Sharp spatially constrained
39 inversion with applications to transient electromagnetic data. *Geophys Prospect* 63:243–255. doi:
40 10.1111/1365-2478.12185
- 41 Waxman MH, Smits LJM (1968) : Electrical Conductivities in Oil-Bearing Shaly Sands. *Soc Pet Eng*

1 J 8:107–122. doi: 10.2118/1863-A

2 Weissmann GS, Fogg GE (1999) : Multi-scale alluvial fan heterogeneity modeled with transition
3 probability geostatistics in a sequence stratigraphic framework. J Hydrol 226:48–65. doi:
4 10.1016/S0022-1694(99)00160-2

5 Zhou H, Gómez-Hernández JJ, Li L (2014) : Inverse methods in hydrogeology: Evolution and recent
6 trends. Adv Water Resour 63:22–37. doi: 10.1016/j.advwatres.2013.10.014

7

8

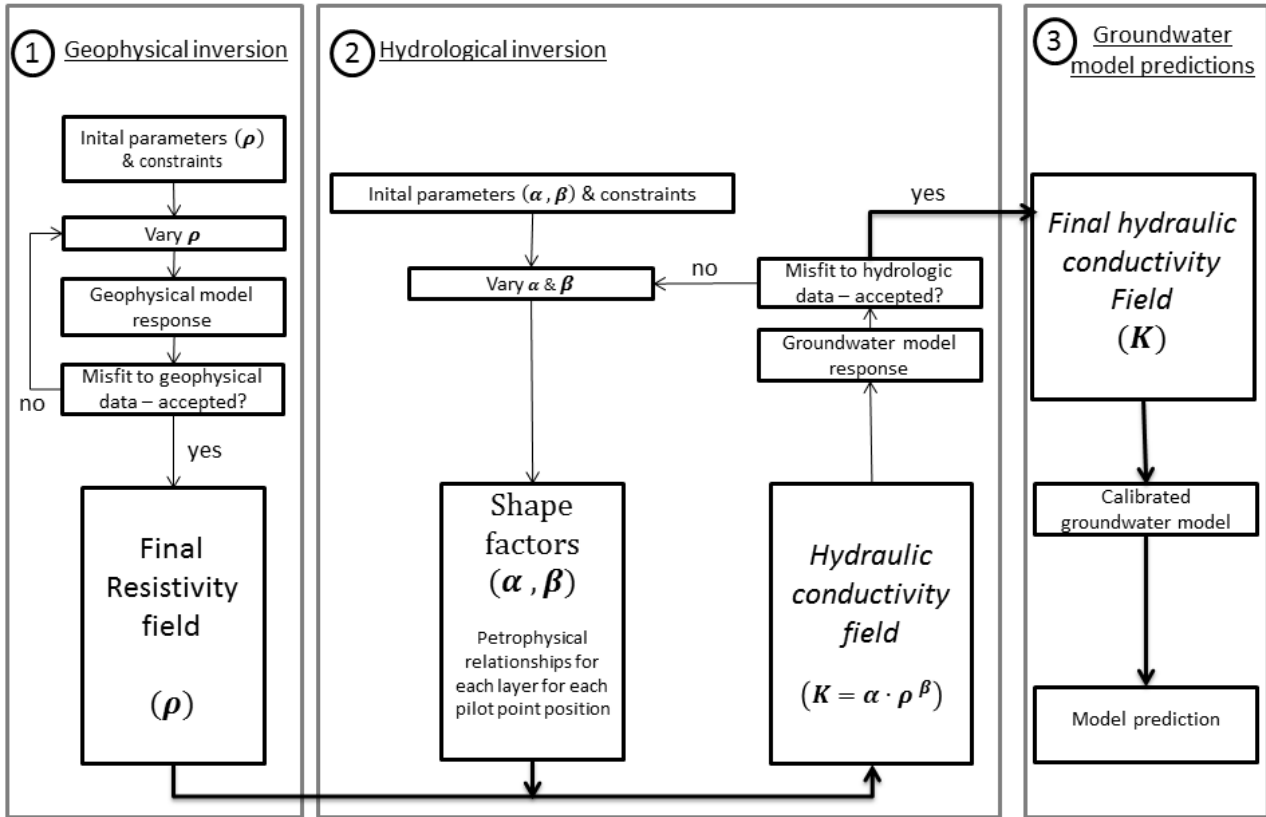
9

1 Table 1. Model structural accuracy comparison for groundwater model using both smooth or sharp
 2 geophysical models and different background noise levels. The results are averaged over the 20
 3 system realizations. A value of 1.0 means that the model’s hydraulic conductivity field is in good
 4 agreement with the reference field; a value of 0.0 means no agreement (see body text for exact
 5 definition of “structural accuracy”).

	Layer 1	Layer 2	Layer 3	Layer 4	Layer 5
SHI-1 Smooth	0.89	0.79	0.56	0.54	0.64
SHI-1 Sharp	0.96	0.91	0.81	0.61	0.48
SHI-3 Sharp	0.96	0.92	0.82	0.64	0.5
SHI-5 Sharp	0.96	0.91	0.78	0.64	0.49
SHI-10 Sharp	0.96	0.9	0.78	0.6	0.46

6

1

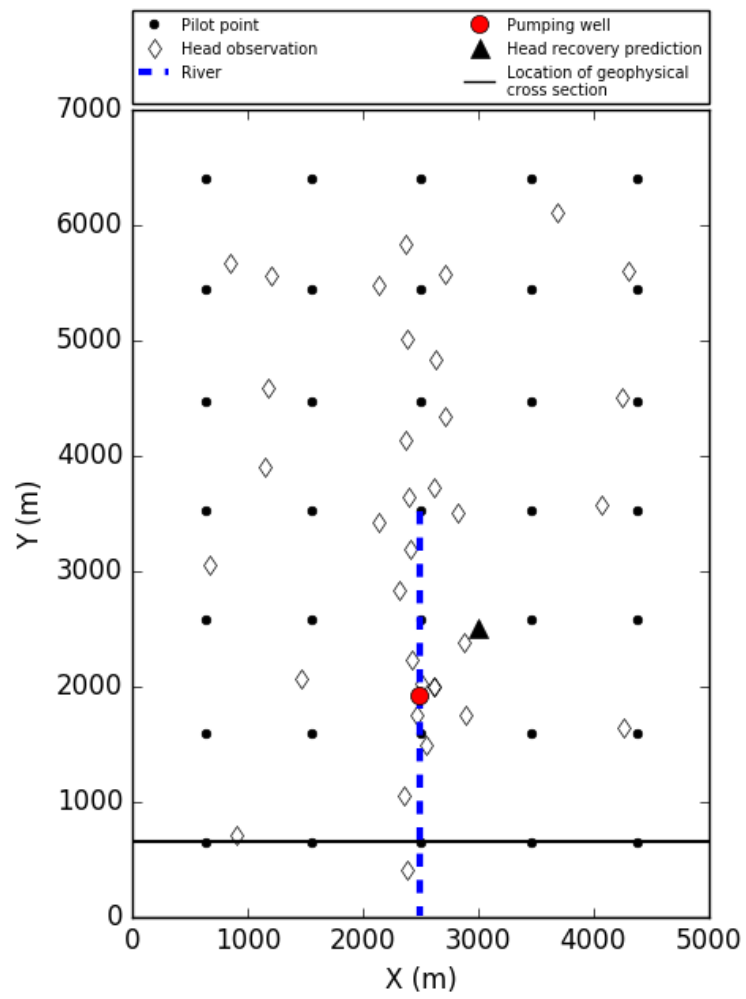


2

3 Figure 1. Conceptual flowchart for the sequential hydrogeophysical inversion. First step (box 1):
4 geophysical inversion. Second step (box 2), groundwater model calibration where shape factors of the
5 petrophysical relationship is estimated using hydrological data. Third step (box 3): The calibrated
6 groundwater model is used for predictive modeling.

7

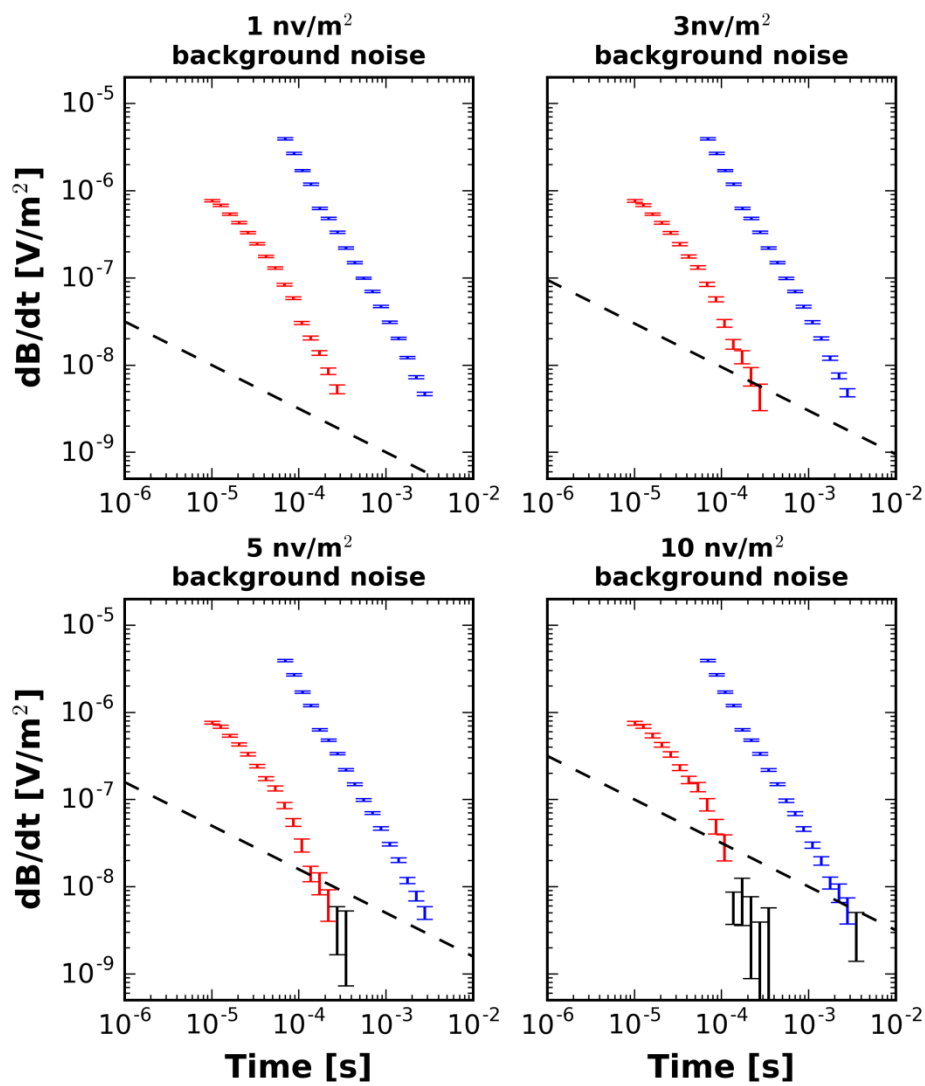
8



1

2 Figure 2. A map of locations of boreholes, a pumping well, pilot points, head recovery prediction and
 3 location of a geophysical cross-section.

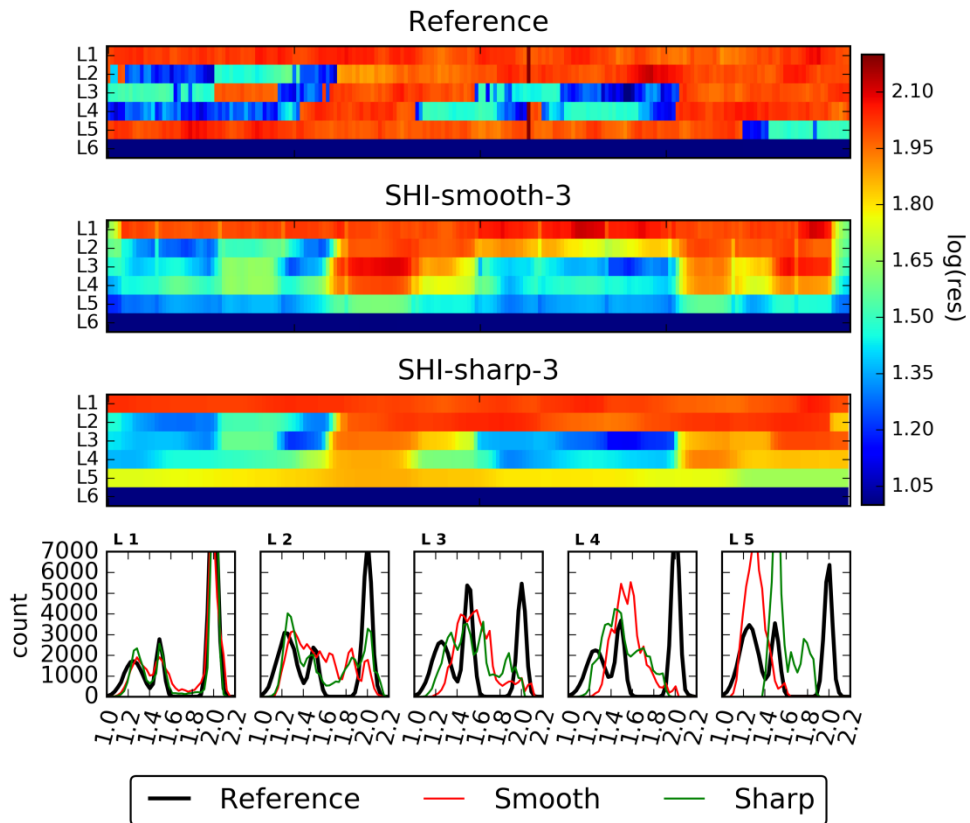
4



1

2 | Figure 3. AEM sounding data corrupted by four levels of background noise. The values on top of each
 3 | subplot corresponds to the noise level at 1 ms and to the b -value in eq. 6. The black dashed curves
 4 | indicate the background noise levels, low and high moment earth responses are illustrated as red and
 5 | blue error bars, respectively, and the black error bars illustrate data which are removed by the data
 6 | processing

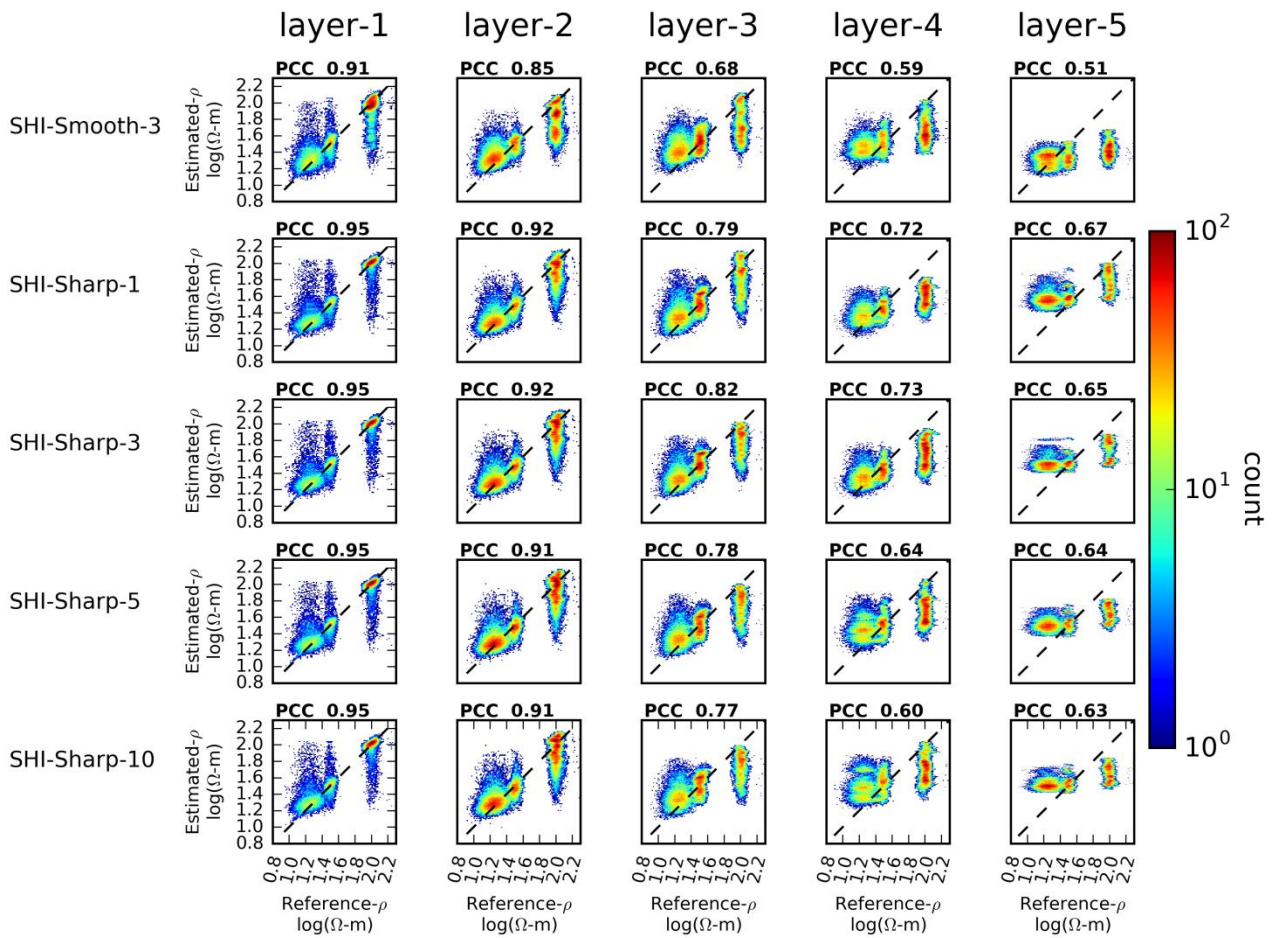
7



1

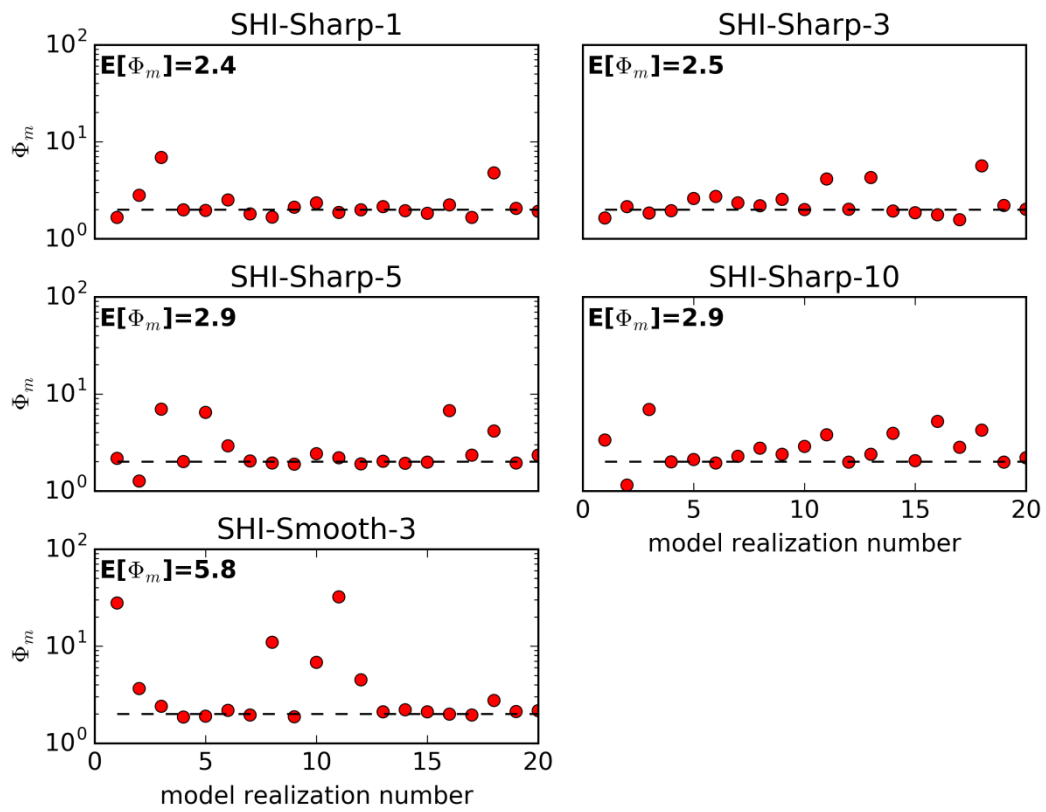
2 Figure 4. The figure shows an East-West cross section of resistivity for the reference system
 3 (realization number 20), and inversion results for Smooth and Sharp inversion, respectively. The last
 4 row shows at histogram of resistivity for each layer. The black curve is the resistivity distribution for
 5 the reference system, the red curve shows the resistivity distribution for the smooth inversion, and
 6 finally the green curve shows the resistivity distribution for the smooth inversion.

7



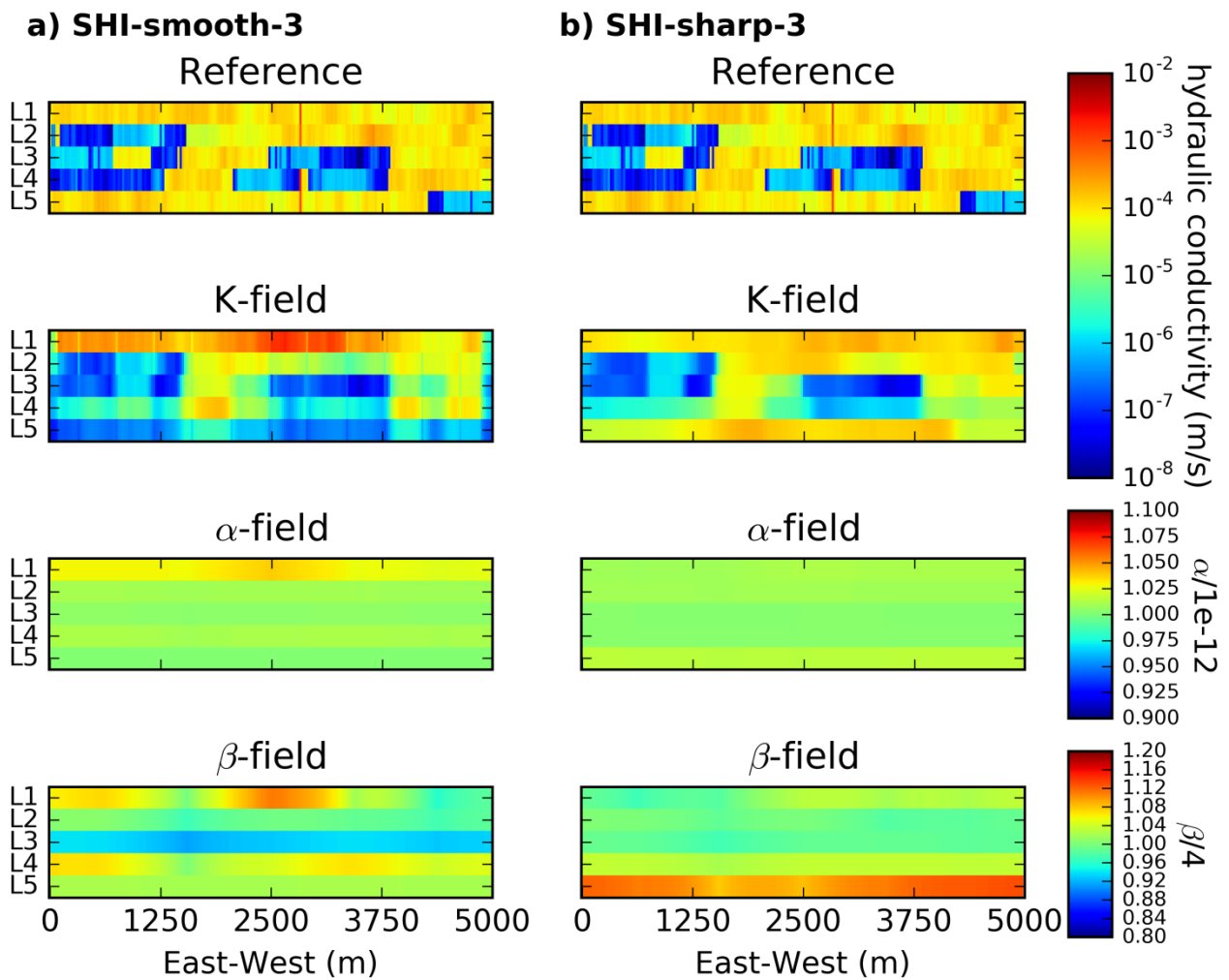
1

2 Figure 5. Scatterplot of true and estimated electrical resistivity field for smooth geophysical inversion
 3 and sharp geophysical inversion for different data quality of the AEM data for model realization
 4 number 20. On top of each window is Pearson correlation coefficient (PCC) calculated.



1

2 Figure 6. Measurement objective function value obtained for the various groundwater model
 3 calibration cases, while $E[\Phi_m]$ is the mean value across all 20 different system realizations. The
 4 dashed line indicates the expected target value for the model calibrations.



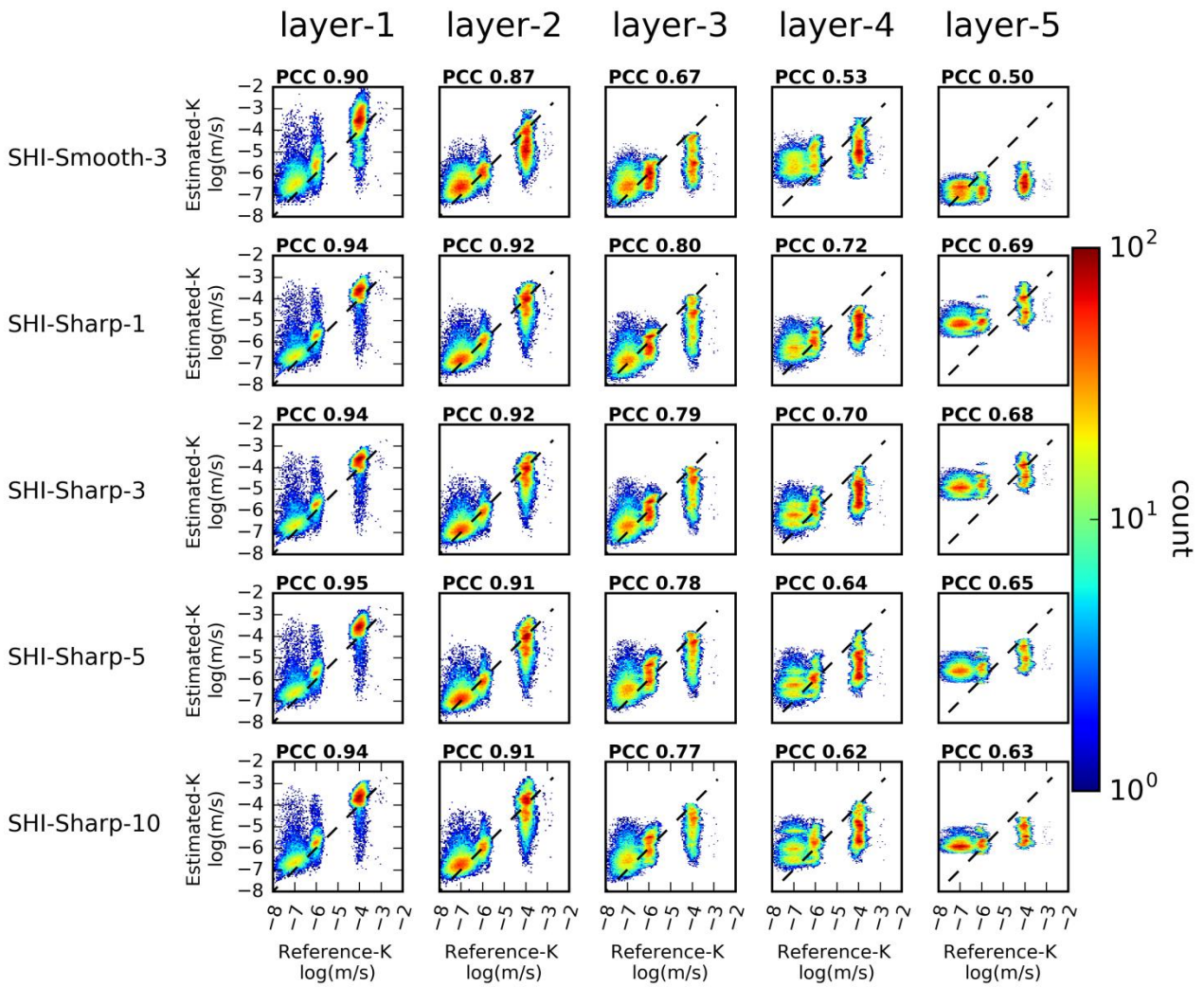
1

2 Figure 7. East-West cross-section for model realization number 20. a) shows the parameters fields for
 3 the SHI-smooth-3 calibrated model. b) Shows the parameters fields for the SHI-sharp-3 calibrated
 4 model. First row shows the reference K-field, second row shows the estimated K-field, third and
 5 fourth row shows shape factors of the petrophysical relationship for alfa and beta, respectively.

6

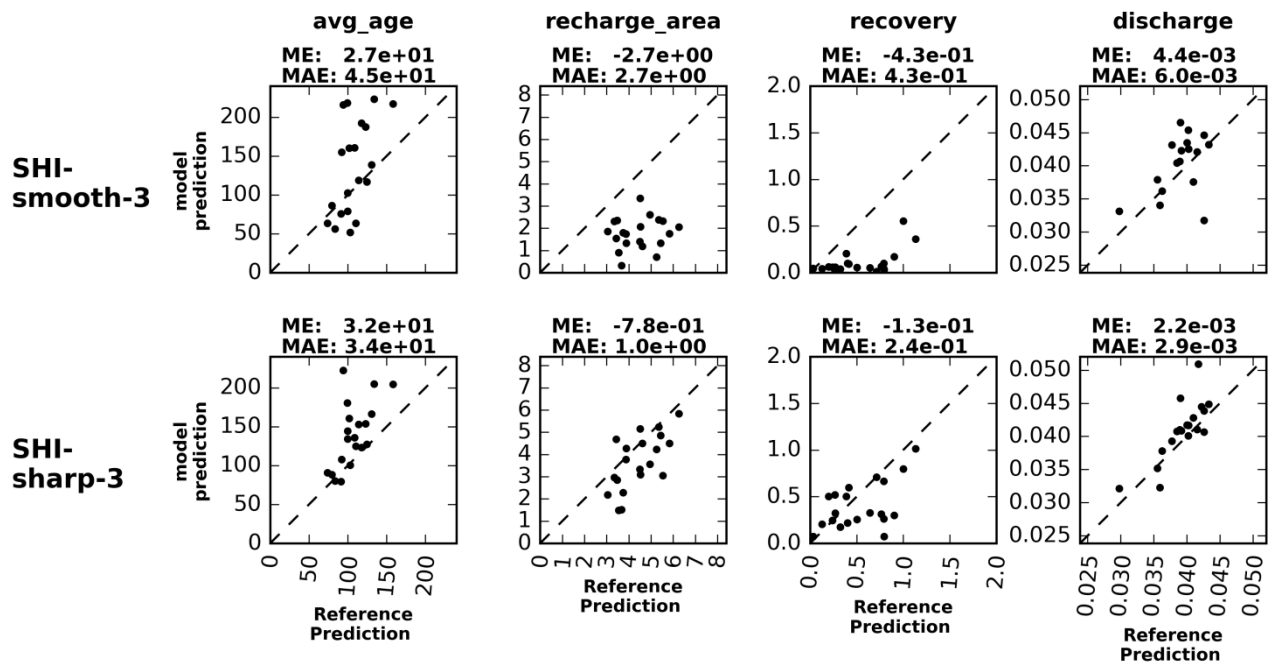
7

8



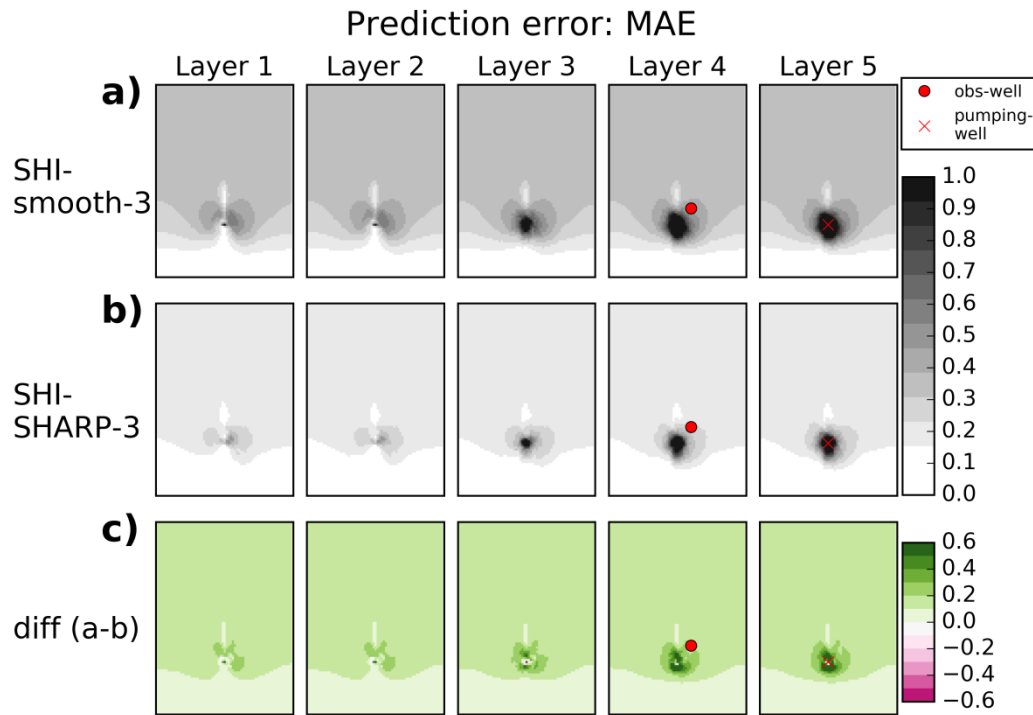
1

2 Figure 8. Scatterplot of true and estimated hydraulic conductivity field for smooth geophysical
 3 inversion and sharp geophysical inversion for different data quality of the AEM data for model
 4 realization number 20. On top of each window is Pearson correlation coefficient (PCC) calculated.



1

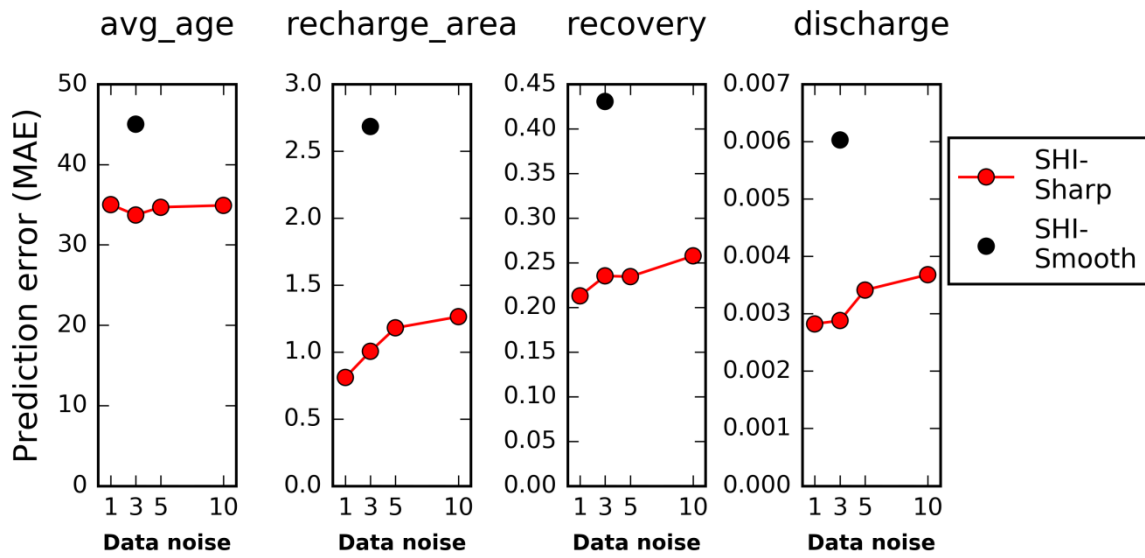
2 Figure 9. Scatter plots of calibrated model prediction versus the reference model prediction using
 3 results from the 20 system realizations. The plots in the first and second -columns isare the average
 4 groundwater age and recharge area, respectively, to of the pumping well. Column three for head, the
 5 second column is for head recovery when pumping has stopped in the observation well shown in
 6 Figure 10, and the fourth third column four is for groundwater discharge to the river after pumping has
 7 stoppedceased, fourth and fifth column is the average age and recharge area to the pumping well. *ME*
 8 and *MAE* are used to quantify the prediction error on basis of the 20 realizations.



1

2 Figure 10. MAE contour map for head recovery prediction. a) For predictions using the SHI-smooth
 3 models. b) For predictions using the SHI-smooth models. c) Difference between maps shown in a)
 4 and b). Red dot marks the location of the observation well for the head recovery prediction shown in
 5 [Figure 9](#). The red cross marks the location of the pumping well.

6



1

2 Figure 11. Prediction error as function of the background noise on the geophysical data. The black dot
 3 is the SHI-smooth models using a background noise level of 3nV/m^2 . The red dots are the SHI-sharp
 4 models as a function of background noise level.